An *in vitro* assay of MCTS1-DENR-dependent re-initiation and ribosome profiling uncover the activity of MCTS2 and distinct function of eIF2D

Romane Meurs[1], Mara De Matos[1], Adrian Bothe[2], Nicolas Guex[3], Tobias Weber[4], Aurelio A. Teleman[4], Nenad Ban[2], David Gatfield[1*]

Affiliations:

[1] Center for Integrative Genomics, University of Lausanne, 1015 Lausanne, Switzerland.

[2] Department of Biology, Institute of Molecular Biology and Biophysics, ETH Zurich, 8093 Zurich, Switzerland.

[3] Bioinformatics Competence Center, University of Lausanne, 1015 Lausanne, Switzerland.

[4] Division of Signal Transduction in Cancer and Metabolism, German Cancer Research Center (DKFZ), Heidelberg, Germany.

[*] Corresponding author

Email addresses: romane.meurs@unil.ch, mara.dematos@unil.ch, adrian.bothe@mol.biol.ethz.ch, nicolas.guex@unil.ch, tobias.weber@dkfz-heidelberg.de, a.teleman@dkfz-heidelberg.de, ban@mol.biol.ethz.ch, david.gatfield@unil.ch

Abstract

Ribosomes scanning from the mRNA 5′ cap to the start codon may initiate at upstream open reading frames (uORFs), decreasing protein biosynthesis. Termination at a uORF can lead to re-initiation, where the 40S subunit resumes scanning and initiates another translation event downstream. In mammals, the noncanonical translation factors MCTS1-DENR participate in re-initiation at specific uORFs, but knowledge of other *trans*-acting factors and uORF features influencing re-initiation is limited. Here, we describe a cell-free re-initiation assay using HeLa cell lysates. Comparing *in vivo* and *in vitro* re-initiation activities on uORF-containing model reporters, we validate that MCTS1-DENR-dependent re-initiation is accurately recapitulated *in vitro*. Using this system and ribosome profiling in cultured cells, we found that knockdown of the homolog eIF2D causes widespread gene expression deregulation unrelated to uORF translation, suggesting distinct functions from MCTS1-DENR. Additionally, we identified MCTS2, encoded by a retrogene copy of *Mcts1*, as an alternative DENR partner that promotes re-initiation *in vitro*, providing a plausible explanation for the striking clinical differences associated with *Denr* vs. *Mcts1* mutations in humans. Our findings on re-initiation and the new assay provide valuable insights and a powerful tool for future research on uORF features and *trans*-acting factors.

Introduction

Upstream open reading frames (uORFs) are abundant, short regulatory elements found within the 5′ UTRs of an estimated 50 % of human transcripts [1]. uORF translation has long been recognised as a mechanism to tune the translation efficiency (TE) of the protein coding sequence (CDS) under physiological and stress conditions [2-5], and several cases of misregulated uORF-dependent translational control have been linked to human diseases including cancer [6-9]. Because uORFs intercept scanning ribosomes and reduce the probability that they engage in initiation downstream, they are generally inhibitory to protein biosynthesis from the CDS. Two main mechanisms are implicated in ensuring that CDS translation can take place nevertheless: first, in a process called leaky scanning, the 43S preinitiation complex can scan across the uORF start codon, thus ignoring the uORF; second, the ribosome can translate the uORF, terminate at its stop codon, and then engage in the process of re-initiation, where the small ribosomal subunit resumes scanning to a downstream start codon [1]. In contrast to canonical initiation, for which many implicated initiation factors and mechanistic details have been identified over the last decades, our understanding of re-initiation has remained incomplete. Thus, large knowledge gaps exist regarding the *trans*-acting protein machinery and to what extent it is shared with canonical initiation, and the *cis*-acting mRNA and uORF sequence requirements that predispose to re-initiation.

A peculiar case of re-initiation-competent uORFs that has been studied contains only a single amino acid – i.e., the start codon – followed immediately by a stop codon (termed '1-aa uORF' or 'start-stop uORF' in the following) [10, 11]. In regular initiation, the initiator-tRNA is positioned in the ribosomal P-site, and on 1-aa uORFs the stop codon is thus already placed in the A-site, ready for termination and without the ribosome ever entering into elongation. Hence, and as shown for eIF3 [12], some canonical initiation factors from the uORF initiation event may likely still be available on the ribosome for subsequent re-initiation. *In vivo*, eIFs have been seen to remain associated with elongating ribosomes for roughly 12 codons, potentially enabling re-initiation after short uORFs but not long uORFs [13].

The heterodimeric, non-canonical initiation factor MCTS1-DENR has been identified as the first, re-initiation-specific translation factor with conserved activity in *Drosophila*, mouse and human [10, 11, 14-17]. *In vitro,* MCTS1-DENR shows the double activity of being able to recruit and release tRNA from the ribosomal P-site [14, 18]. The yeast orthologues, Tma20-Tma22, appear to mainly function in post-termination tRNA removal

67 and 40S ribosome recycling rather than as promoters of re-initiation [19, 20]. In animal model systems, DENR
68 loss-of-function followed by ribosome profiling has been used to identify CDS translation efficiency changes
69 indicative of altered re-initiation, thus identifying likely direct MCTS1-DENR targets [10, 11, 17, 21]. These
70 studies revealed that only a small fraction of all uORF-containing transcripts undergo MCTS1-DENR-
71 dependent re-initiation and, while start-stop uORFs are highly represented among targets, longer uORFs were
72 associated with MCTS1-DENR-dependent re-initiation as well. As a first hint towards the selectivity of
73 MCTS1-DENR for certain uORFs, an enrichment for specific penultimate uORF codons was observed among
74 targets in HeLa cells [21] and in yeast [20], leading to the hypothesis that MCTS1-DENR removes deacylated
75 P-site tRNA from the terminated ribosome and that the efficiency of this process may be tRNA-specific.
76 The protein eIF2D is a close homologue of MCTS1-DENR, containing the same domains encoded on a single
77 polypeptide. Like MCTS1-DENR, eIF2D (then still under the name LGTN, for Ligatin) was initially identified
78 as a recycling and initiation factor based on its *in vitro* activities [14], and the yeast orthologue, Tma64, has
79 been noted for its role in 40S subunit recycling, too [19]. Due to these similarities, eIF2D is frequently referred
80 to as a re-initiation factor as well, and evidence for comparable functions of MCTS1-DENR and eIF2D on
81 uORFs come from studies of *Atf4* regulation in *Drosophila* and in HeLa cells [21, 22]. However, eIF2D does
82 not regulate an MCTS1-DENR-dependent synthetic model start-stop uORF *in vivo* [11], suggesting that the
83 two factors may be active on distinct sets of uORFs and transcripts. Furthermore, it has recently been reported
84 that the single knockout of yeast Tma64/*Eif2d* does not recapitulate the 40S recycling defect observed in the
85 single knockout of Tma22/*Denr* [20]. Therefore, it would appear that the involvement of eIF2D in re-initiation
86 and/or recycling still needs to be formally established.
87 In this study, we combined ribosome profiling, *in vivo* reporter assays and experiments using a cell-free
88 translation system to investigate MCTS1-DENR- and eIF2D-dependent re-initiation. Using the *in vivo* and *in*
89 *vitro* re-initiation assays, we measured the fluxes of ribosomes on the 5′ UTRs of two identified DENR-
90 dependent model transcripts, *Klhdc8a* and *Asb8*, and addressed the effect of penultimate codon identity.
91 Ribosome profiling from DENR and eIF2D loss-of-function cells pointed at different and distinct roles for the
92 two factors in gene expression regulation and, importantly, indicated that eIF2D does not act as a general uORF
93 re-initiation factor. Finally, we identified MCTS2 as an alternative DENR heterodimerisation partner *in vivo*
94 whose activity in re-initiation we analysed and validated in our *in vitro* assay.

Results

Upstream open reading frame-containing transcripts *Klhdc8a* and *Asb8* are regulated by DENR *in vivo* and suitable for model reporter design.

To gain insights into mechanism and targets of DENR-dependent re-initiation, we first identified uORF-containing transcripts for which CDS translation was altered after shRNA-mediated knock-down of *Denr* in murine NIH/3T3 cells (**Figure 1A**). To this end, we carried out ribosome profiling (Ribo-seq) and RNA-seq from *Denr* shRNA-treated cells, as well as from two different control-treated cells, exposed either to scramble (Scr) shRNA or to non-functional (nf) *Eif2d* shRNA that did not cause any knockdown (**Figure 1A**). From the obtained data, we calculated translation efficiencies (TEs, ratio CDS footprints to RNA) transcriptome-wide, thus identifying 223 and 6 transcripts, respectively, with significantly reduced and increased TE (applying FDR-corrected $p < 0.1$) (**Figure 1B;** Supplementary Table S1). The strong bias for reduced TEs was in line with our expectations for direct targets of a factor facilitating re-initiation on the CDS after uORF translation, and with previous findings [17, 21]; we further noted that the annotated 5′ UTRs of transcripts with reduced TE were significantly longer than would be expected from the transcriptome-wide distribution of 5′ UTR lengths (**Figure 1C**), compatible with increased uORF content. Indeed, annotation of translated uORFs from the footprint data showed strong enrichment among the DENR-responsive transcripts (**Figure 1D**). The lengths of the identified uORFs showed a broad distribution, with 1-aa/start-stop uORFs being the most abundant species but many longer, elongating uORFs found on the DENR-responsive transcripts as well (**Figure 1E**). We selected two transcripts to design re-initiation reporters, representing an elongating uORF (*Klhdc8a*, *Kelch domain containing 8A*; 13 amino acid uORF) and a start-stop uORF (*Asb8, Ankyrin repeat and SOCS box-containing 8*) (**Figure 1B**). Both mRNAs presented significantly reduced TE upon *Denr* knockdown (decrease by ~70 % for *Klhdc8a* and by ~30 % for *Asb8*; **Figure 1G**) and, moreover, their 5′ UTRs contained only one strongly translated, AUG-initiating uORF (**Figure 1F** and **Supplementary Figure S1A, B**) which is conserved in human and other mammals (**Supplementary Figure S1C, D**). We then confirmed that *Denr* KO in human HeLa cells indeed led to a strong downregulation of endogenous KLHDC8A protein as evaluated by immunoblot analysis using specific antibodies (**Figure 1J**). The lack of functional antibodies against mouse or human ASB8 precluded a similar analysis for this protein.

122 We first used the *Klhdc8a* 5′ UTR (and the first codons of its CDS, fused in-frame to firefly luciferase) to
123 establish a set of three different reporter genes that would allow us to estimate re-initiation and leaky scanning
124 rates (**Figure 1H**). Thus, the *WT uORF* reporter contained the full, unmodified *Klhdc8a* 5′ UTR. Mutating the
125 uORF start codon (*no uORF* reporter) allowed us to quantify luciferase signal when no inhibitory uORF is
126 present. A third reporter contained a mutated uORF stop codon, which extended the uORF coding sequence
127 all the way into the luciferase CDS, but in a different frame (*overlapping uORF* reporter). Thus, this reporter
128 would give luciferase signal only through leaky scanning of ribosomes across the uORF start codon. After
129 reporter delivery into HeLa cells (via lentiviral constructs that also contained a Renilla luciferase reporter for
130 internal normalisation across samples), re-initiation signal can be extracted from the individual reporter
131 readouts as shown in **Figure 1I**. The relative reduction of signal from *no uORF* to *WT uORF* reporters thus
132 represents the overall inhibitory activity of the uORF, with remaining signal corresponding to the sum of leaky
133 scanning- and re-initiation-mediated reporter translation. By further subtracting the *overlapping uORF* reporter
134 signal that derives from leaky scanning, re-initiation is quantified. Using WT and *Denr* KO HeLa cells (**Figure**
135 **1J**), this assay indicated strong inhibition by the *Klhdc8a* uORF, and remaining signal that was largely DENR-
136 dependent, as well as very low leaky scanning rates (**Figure 1I**). This data allowed us to propose a model of
137 how ribosomal fluxes occur on the *Klhdc8a* reporter transcript *in vivo* (**Figure 1K**). Our analyses suggest that
138 ~98% of ribosomes initiate on the uORF and only ~2% undergo leaky scanning. Of the uORF ribosomes about
139 19% re-initiate on the main CDS, a process that is largely DENR-dependent.
140 We concluded that translation of endogenous and reporter-encoded KLHDC8A was highly re-initiation-
141 dependent and that our system based on three reporters, together with the use of WT vs. *Denr* KO cells, allowed
142 the quantification of DENR-dependent re-initiation *in vivo*.

143 **An *in vitro* re-initiation assay recapitulates regulation and ribosome fluxes observed *in vivo*.**
144 Next, we set out to establish an *in vitro* assay that could recapitulate re-initiation. To this end, we prepared
145 translation-competent extracts from HeLa cells, essentially adapting a recently reported protocol based on
146 detergent-free cell lysis applying reproducible shearing forces via a dual centrifugation step [23] (**Figure 2A**).
147 Under the gentle lysis conditions used, a sizeable proportion of cells remained intact (**Figure 2B**, pellet
148 fraction), yet we found the supernatant to reproducibly recover highly translation-competent lysate that also
149 contained the three proteins of interest for our study (MCTS1, DENR, eIF2D) (**Figure 2B**). Initial tests

150 revealed that during the *in vitro* translation reaction, eIF2α became phosphorylated at Ser51 (**Figure 2C**), a
151 modification that is associated with decreased initiation rates leading to low translational output. As previously
152 reported [23, 24], the addition of recombinant GADD34Δ1-240 greatly counteracted Ser51 phosphorylation
153 (**Figure 2C**). Indeed, in the absence of GADD34Δ1-240, luciferase signals that were obtained in *in vitro*
154 translation assays for various *in vitro* transcribed, capped and polyadenylated reporter RNAs were >50 %
155 reduced as compared to reporter signals in the presence of recombinant GADD34Δ1-240 (**Figure 2D**). As
156 default condition in our experiments, we hence added recombinant GADD34Δ1-240 to all reactions. Finally,
157 we further optimised the *Klhdc8a*-based reporters by shortening the 5′ UTR from its original ~650 nt down to
158 ~180 nt, retaining the larger uORF environment yet removing far upstream 5′ UTR sequence (**Supplementary**
159 **Figure S2A**). These short *Klhdc8a* 5′ UTR reporters showed strongly increased signals in our assays
160 (**Supplementary Figure S2B**), in line with the notion that 5′ UTR length generally anticorrelates with CDS
161 translation efficiency (e.g. [13, 25]).
162 First, we carried out the *in vitro* translation assays on the set of *Klhdc8a* reporters (no uORF, WT uORF,
163 overlapping uORF), using HeLa extracts prepared from both wild-type and *Denr* KO cells. These experiments
164 revealed clear uORF- and DENR-dependence (**Figure 2E**, left side; identical outcomes for "long *Klhdc8a* 5′
165 UTR" reporter, see **Supplementary Figure S2C**), closely resembling our observations *in vivo* (**Figure 1I**).
166 The calculated ribosomal fluxes showed excellent correspondence as well (**Figure 2F**). In particular, the uORF
167 strongly impeded CDS expression with very low rate of leaky scanning (1%). Re-initiation-mediated reporter
168 expression (11%) was quantitatively slightly lower than *in vivo* (19%, see **Figure 1K**), yet remained highly
169 DENR-dependent (i.e., in *Denr* KO extracts the signal from the 'WT uORF' reporter was close to the leaky
170 scanning signal from the 'overlapping uORF' reporter). Importantly, this lack of re-initiation in *Denr* KO
171 extracts could be fully rescued through complementation with recombinant MCTS1-DENR (**Figure 2E**, right),
172 confirming the direct involvement of these proteins in re-initiation *in vitro*. Note also that in *Denr* KO, MCTS1
173 is co-depleted (**Figure 1J**) as a result of its instability in the absence of its binding partner (as previously
174 observed in [21, 26]), making a rescue with both proteins necessary. We concluded that our *in vitro* assays
175 showed very good correspondence with re-initiation parameters observed *in vivo*.
176 Next, we assayed *in vitro* the start-stop uORF-containing *Asb8* reporter set (**Figure 2G**). These experiments
177 revealed that this uORF was rather permissive to leaky scanning, likely due to poor Kozak context of its start

178 codon; in particular, given that all stop codons (TGA, TAA, TAG) begin with a T nucleotide, start-stop uORFs
179 by default have a (suboptimal) T in Kozak sequence +4 position. The lower efficiency of inhibition by the
180 *Asb8* uORF (as compared to the *Klhdc8a* uORF) was in line with the translation efficiencies measured *in vivo*
181 by Ribo-seq (**Figure 1G**). According to our calculations (**Figure 2H**), 58% of ribosomes underwent leaky
182 scanning and 42% engaged in uORF translation. About two-thirds of uORF termination events led to re-
183 initiation at the CDS and the remaining one-third did not (29% vs. 13%). Re-initiation was mostly MCTS1-
184 DENR-dependent, as judged from the signals obtained in *Denr* KO extracts and from recombinant MCTS1-
185 DENR rescue (**Figure 2G**).
186 MCTS1-DENR selectivity for certain uORFs has been linked to specific penultimate codons [19][21]. The
187 *Klhdc8a* uORF terminates with the sequence '… GTG(Val) TAG(Stop)', yet penultimate GTG was not
188 observed as specifically associated with DENR-dependence previously [21]. In order to test penultimate codon
189 influence in our assay, we tested reporters in which the GTG(Val) was mutated to GTC(Val) (among the
190 reported significantly depleted penultimate codons in DENR-dependent uORFs [21]) and to GCG(Ala) (most
191 strongly and significantly enriched in DENR-dependent uORFs according to [21]) (**Figure 2I**). We found that
192 the inhibitory impact of the uORF and re-initiation rates were only weakly affected by these codon changes;
193 in particular, re-initiation was lower (non-significant) than in wild-type codon constructs and it still remained
194 strongly DENR-dependent. Interestingly, in the depleted penultimate codon case, GTC(Val), DENR-
195 dependence of re-initiation was reduced, yet overall re-initiation capacity still intact. This observation is
196 compatible with the idea that the depleted penultimate codon is able to partially decouple the re-initiation
197 process from its dependence on these particular re-initiation factors.
198 Next, we examined *Asb8* reporter variants, converting the 1-aa uORF to a 2-aa uORF (and thus from start-stop
199 to elongating uORF) and testing different penultimate codons. Thus, we inserted either a TGT(Cys), which is
200 (according to [21]) the only significantly enriched penultimate codon starting with 'T' (hence preserving the
201 +4 Kozak context of the start codon), or GCG(Ala), which is a highly enriched codon and additionally
202 improves the Kozak context for uORF initiation (**Figure 2J**). In the *in vitro* translation assays, GCG insertion
203 indeed led to strongly decreased leaky scanning rates, converting the weakly translated 1-aa uORF to a strongly
204 translated 2-aa uORF (**Figure 2J**, right), compatible with the improved Kozak consensus associated with the
205 +4 position 'G'. Lengthening the uORF with TGT(Cys) had little consequences on leaky scanning and overall

206 re-initiation rate, yet DENR-dependence appeared reduced (**Figure 2J**, middle). We concluded that re-
207 initiation rates were not *per se* different between start-stop and elongating uORFs, but the DENR-dependence
208 of re-initiation was modulated, which is in agreement with the reported preferential MCTS1-DENR regulation
209 of start-stop uORFs [11, 21].

210 **Phospho-eIF2α levels only mildly affect re-initiation rates of *Klhdc8a* and *Asb8* reporters.**

211 Phosphorylation of eIF2α is key to the integrated stress response (ISR) that lowers bulk translation initiation
212 and promotes preferential translation of stress-related mRNAs through a mechanism that involves uORFs, re-
213 initiation and start codon selection [27]. The current model deduced from studying transcripts such as
214 *Atf4/Gcn4* suggests that after uORF termination, the re-scanning 40S subunit becomes rapidly re-initiation-
215 competent when non-phosphorylated (active) eIF2α is abundant. This leads to translation of a relatively close
216 (87 nt) downstream, second uORF rather than the CDS that is more distant (184 nt). However, when p-eIF2α
217 levels are high, the probability of recruiting active eIF2α in time for the second uORF is lower, and re-initiation
218 will more often occur further downstream, on the CDS. Recent work has highlighted the importance of both
219 MCTS1-DENR and eIF2D for *Atf4* CDS translation [21, 22]. Despite these links, whether eIF2α activity is a
220 rate-limiting factor for MCTS1-DENR-mediated re-initiation *per se*, and to what extent the reported effects
221 are a consequence of global initiation decrease, remains unclear. We reasoned that our well-controlled *in vitro*
222 system would allow us to address such questions.

223 We thus carried out our assays in the presence vs. absence of GADD34Δ1-240, which led to low and high
224 Ser51 phosphorylation levels of eIF2α, respectively (**Figure 2C**). The level of Ser51 phosphorylation occurring
225 in the absence of GADD34Δ1-240 was even higher than that seen after a standard ISR induction protocol by
226 tunicamycin treatment of cells (**Supplementary Figure S3A**). For the *Klhdc8a* reporters, absolute signals were
227 significantly reduced in the absence of GADD34Δ1-240 as expected (analogous to experiments in **Figure 2D**),
228 yet after normalisation to the (likewise reduced) Renilla luciferase signal, the observed levels of leaky scanning
229 (slightly up) and uORF-mediated inhibition (slightly down), the re-initiation rate (slightly down) and its
230 DENR-dependence (up), and the calculated ribosomal fluxes were highly similar between both conditions
231 (**Figure 3A, B**). We concluded that in the *Klhdc8a* reporter *in vitro* experiments, the availability of non-
232 phosphorylated eIF2α was not *per se* a strongly rate-limiting step for re-initiation. On the *Asb8* reporter –
233 where the intercistronic distance between uORF and CDS is very short (17 nt, as compared to 73 nt in *Klhdc8a*)

234 – we found overall more variability in the experimental outcomes in the absence of GADD34Δ1-240 (**Figure**
235 **3C, D**). We observed a tendency to increased leaky scanning and reduced re-initiation (both non-significant).
236 In an *in vivo* experiment on the *Klhdc8a* reporter set, combined with tunicamycin treatment, we also observed
237 a weak reduction in re-initiation rate (**Supplementary Figure S3B, C**) and validated that under these
238 conditions the translation of positive control reporters carrying the 5′ UTRs of *Atf4* and *Atf5* upstream of
239 luciferase were indeed upregulated (**Supplementary Figure S3D**). Taken together, these results suggest that
240 eIF2α levels are only moderately limiting for re-initiation.

241 **Limited evidence for a role of eIF2D in re-initiation *in vivo* and *in vitro*, pointing to uORF-independent**
242 **cellular functions in gene expression regulation.**

243 Next, we extended our analyses to the close MCTS1-DENR homologue, eIF2D, which contains the same
244 domains encoded as a single polypeptide, linked by an additional WH domain (**Figure 4A**). The high similarity
245 between the proteins, in addition to the findings that the yeast orthologues show shared activities, has led to
246 the assumption that the homology in mammals extends to their function. To test this hypothesis, we
247 downregulated eIF2D using specific shRNAs (**Figure 1A**) and carried out Ribo-seq and RNA-seq identically
248 to the experiment in *Denr*-depleted cells shown in **Figure 1B**. For a first comparison between the two
249 genotypes, i.e. *Eif2d*-depleted and *Denr*-depleted, we evaluated in a transcriptome-wide fashion the relative
250 ribosome distribution between mRNA 5′ UTR and CDS sequences. This measure is expected to increase when
251 a re-initiation factor is depleted because ribosomes are selectively lost from CDS sequences but will still
252 translate uORFs when re-initiation in inhibited [17]. Indeed, the distribution of the changes seen for 5′ UTR-
253 to-CDS footprint ratios between *Denr* shRNA-treated cells vs. control cells was strongly shifted to the positive
254 (**Figure 4B**), indicating globally detectable ribosome redistribution in the absence of MCTS1-DENR,
255 consistent with previous findings [17]. By contrast, the shift was considerably smaller in the cells that had been
256 treated with *Eif2d* shRNAs (**Figure 4B**). Next, we carried out an analysis identical to that applied to *Denr*
257 knockdown cells in **Figure 1B**, to determine the effects induced by *Eif2d* depletion at the level of CDS
258 translation efficiencies (**Figure 4C**). This analysis, too, revealed strikingly different transcriptome-wide effects
259 between the homologues. We thus detected much fewer transcripts with a decreased TE upon *Eif2d* knockdown
260 (n = 78, with FDR-corrected $p < 0.1$; Supplementary Table S2) (**Figure 4C**) as compared to *Denr* knockdown
261 cells (n = 223) (**Figure 1C**), and the overlap between the two sets was minimal (**Supplementary Figure S4A,**

262 **B**). Moreover, the mRNAs with low TE in *Eif2d*-depleted cells tended to have short 5′ UTRs (**Supplementary**
263 **Figure S4C**) and they were not enriched for translated uORFs (**Figure 4D**). We also noted that many of the
264 translationally affected transcripts were highly abundant, including >25 mRNAs encoding for ribosomal
265 proteins and general translation machinery (**Supplementary Figure S4D, E**). Particularly strong consequences
266 of eIF2D loss-of-function were evident for RNA abundances, with a large number of mRNAs significantly up
267 (n = 460) and downregulated (n = 617) (**Figure 4C**) and, here, abundant transcripts were overrepresented as
268 well (**Supplementary Figure S4F**) and associated with cellular processes such as the cell cycle and translation
269 (**Supplementary Figure S4G, H**). Alterations to the cell cycle could indeed be further validated as a robust
270 phenotype following eIF2D loss-of-function (**Supplementary Figure S4I**). Taken together, these findings
271 suggested that, first, the knockdown of *Eif2d* was phenotypically highly consequential as judged by the
272 widespread gene expression reprogramming that it induced. However, second, it would seem that the primary
273 activity of eIF2D may not lie in regulating the re-initiation of uORF-containing transcripts.
274 To further investigate the above observations on potential eIF2D targets, we selected several candidate
275 transcripts to test if their TE regulation was 5′ UTR-mediated. Of these, *Cenpa*, *Ndc80*, *Med23* and *Rps20* were
276 picked as candidate mRNAs with low TE from **Figure 4C**. We also included *Hoxa3*, which has been identified
277 as a *bona fide* eIF2D-regulated mRNA in a previous study [28]. According to the published findings, eIF2D is
278 implicated in uORF-mediated inhibition, rather than in re-initiation, of *Hoxa3* CDS translation. Indeed, our *in*
279 *vivo* data confirmed *Hoxa3* CDS TE up-regulation upon *Eif2d* depletion (**Figure 4E**; note that *Hoxa3* is very
280 lowly expressed in our cells and did not feature among the significantly changed TE transcripts in **Figure 4C**,
281 but the differences were statistically significant in the direct comparison of TEs shown in **Figure 4E**). *In vivo*
282 luciferase reporter assays using the 5′ UTRs of the selected endogenous candidate transcripts did not reveal
283 significant regulation by eIF2D (**Figure 4F**). We also analysed *Klhdc8*a (endogenous and 5′ UTR reporter),
284 but we found no indication that eIF2D was involved in its re-initiation *in vivo* (**Figure 4E, F**). Endogenous
285 *Asb8* showed an increase in translation efficiency upon *Eif2d* depletion (**Figure 4E**), contrasting the effect seen
286 upon *Denr* depletion.
287 We next tested the outcome of eIF2D loss-of-function and rescue in our *in vitro* assay. In lysates from *Eif2d*
288 KO HeLa cells (**Figure 1J**), no difference in re-initiation activity or leaky scanning was detectable for the *Asb8*
289 reporter (**Figure 4G**). By contrast, for the *Klhdc8a* reporter, re-initiation rates in *Eif2d* KO lysates were reduced

290 by about half (**Figure 4H**). However, neither recombinant eIF2D nor recombinant MCTS1-DENR were able
291 to fully rescue the low signal obtained with the WT uORF reporter in *Eif2d* KO lysates (**Figure 4H**). These
292 observations were most compatible with the model that lower re-initiation signal was an indirect effect of
293 eIF2D loss, e.g. due to secondary effects related to the widespread gene expression reprogramming seen in
294 **Figure 4C**. Thus, we would not expect indirect effects to be rescuable *in vitro*, whereas a direct role in the re-
295 initiation process itself should be rescued by adding the needed re-initiation factor as a recombinant protein.
296 In *Eif2d* knockout extracts, MCTS1-DENR is abundant and may mask the re-initiation function of eIF2D. To
297 address this possibility, we carried out two experiments. First, using re-initiation-deficient *Denr* KO extracts
298 and recombinant eIF2D, we were indeed able to partially rescue re-initiation activity (**Figure 4I**), although not
299 as efficiently as with recombinant MCTS1-DENR (compare with **Figure 2E**). Second, we used *Denr* + *Eif2d*
300 double knockout cell lysates. *In vitro* translation reactions in these extracts showed reduced re-initiation
301 activity (**Figure 4J**, left) that was very similar to *Denr* single knockouts (**Figure 2E**). Addition of recombinant
302 MCTS1-DENR showed the expected rescue (**Figure 4J**, right) and, interestingly, also recombinant eIF2D
303 partially rescued under in these conditions, i.e. in the absence of MCTS1-DENR (**Figure 4J**, middle). Taken
304 together, these results indicate that eIF2D is likely not an essential component of the re-initiation machinery
305 *in vivo* (**Figure 4C**) and *in vitro* (**Figure 4H**). However, when MCTS1-DENR is absent, adding high
306 concentrations of eIF2D (0.5 μM) can partially compensate for MCTS1-DENR loss. Thus, it is a probable
307 scenario that eIF2D has in principle retained some shared activity with MCTS1-DENR, but its main cellular
308 functions seem to lie outside of uORF re-initiation.
309 Finally, it is also possible that eIF2D is active in re-initiation in a conditional fashion; in particular upon
310 induction of the integrated stress response that leads to unavailability of eIF2α, eIF2D may be able to deliver
311 initiator-tRNA to the 40S ribosome. We addressed this possibility by carrying out *in vitro* translation in *Eif2d*
312 knockout extracts (without/with recombinant eIF2D rescue) in the absence of GADD34Δ1-240 (**Figure 4K**).
313 Also under these conditions, we observed the (most likely) indirect/secondary effects of eIF2D loss that could
314 not be rescued by recombinant eIF2D, and the experiment revealed no further indications for a specific re-
315 initiation role of eIF2D.

316 **Identification of MCTS2 as a functional DENR heterodimerization partner.**

317 It has been observed that MCTS1 and DENR are mutually dependent on each other for protein stability [21,
318 26], giving rise to the idea that they act as obligate heterodimers. However, closer inspection of the available
319 cell culture data would suggest that the depletion of MCTS1 in *Denr* KO cells is stronger than the depletion
320 of DENR in *Mcts1* KOs [21]; moreover, *in vivo* phenotypes in mouse neuronal migration are stronger upon
321 DENR loss than MCTS1 loss [29]. These findings could indicate that DENR is indeed an obligatory component
322 of the heterodimer, but that it can interact with and be stabilised by alternative heterodimerization partners as
323 well. To obtain insights into this hypothesis, we sought to purify DENR-interacting proteins by a co-
324 immunoprecipitation and mass-spectrometry approach. Using CRISPR gene editing, we modified the
325 endogenous *Denr* locus in NIH/3T3 cells such that it expressed DENR protein with a C-terminal tag suitable
326 for immunoprecipitation via a 3×FLAG sequence as well as for degron-mediated protein depletion via the
327 dTAG / dTAG-13 degrader system [30] (**Figure 5A**). Genotyping indicated successful modification of both
328 alleles in selected cell clones (**Figure 5B**) and immunoblot analysis validated the functionality of the degron
329 system (**Figure 5C**). We then analysed by mass-spectrometry the proteins enriched in FLAG-IP performed on
330 extracts from control-treated vs. dTAG-13-treated cells (**Figure 5D**). The two most strongly enriched co-
331 purifying proteins were MCTS1 and MCTS2. This finding indicates that DENR assembles into two distinct
332 heterodimeric complexes, MCTS1-DENR and MCTS2-DENR. *Mcts2* is a paralog and retrogene copy of *Mcts1*
333 that has been noted for its transcription from an imprinted gene region in mouse and humans, with predominant
334 expression from the paternal allele [31]. A recent study on human *Mcts1* deficiency and associated disease
335 phenotypes has speculated on redundancy with *Mcts2*, yet based on reporter assays and other analyses, it came
336 to the conclusion that this paralog was largely non-functional [32]. By contrast, our interaction data collected
337 from endogenous proteins suggests that both MCTS paralogs form *bona fide* heterodimers with DENR. The
338 *Mcts1* and *Mcts2* coding sequences differ at 81 individual nucleotide positions that are distributed quite evenly
339 across the overall CDS of 546 nt (**Supplementary Figure S5A**), allowing to unambiguously assign RNA-seq
340 reads and Ribo-seq footprints to the two paralogous sequences. We could thus compare the expression of the
341 *Mcts* paralogs, which indicated higher levels of *Mcts2* than *Mcts1* in our cells (**Figure 5E**). These findings
342 strongly indicate that MCTS2 is a relevant interaction partner of DENR besides MCTS1.
343 Human and mouse MCTS1 protein sequences are identical apart from one leucine to isoleucine substitution at
344 amino acid position 30 (**Figure 5F**). In MCTS2, divergence to MCTS1 can be found at 14 positions when

345 aligning mouse, rat, human and macaque protein sequences, with 4 substitutions common to MCTS2 across
346 species and other changes specific to the analysed rodents or primates (**Figure 5F**). Using available structural
347 data from *in vitro* reconstituted MCTS1-DENR in complex with the 40S ribosome, initiator-tRNA and a viral
348 model RNA [33], we found that MCTS2-specific amino acid changes affected positions that cluster all in the
349 same region of the fold but outside of the interaction surface between MCTS1-DENR and also outside of that
350 between MCTS1-DENR and the 40S ribosomal subunit (**Figure 5G**). Hence, the capacity of MCTS2 vs.
351 MCTS1 to interact with DENR, and of MCTS2-DENR vs. MCTS1-DENR to interact with 40S can be expected
352 to be comparable. However, the substitutions – of which in particular the change at amino acid position 75
353 from glutamate (negative charge) in MCTS1 to lysine (positive charge) in MCTS2 (**Figure 5F**) would have
354 the potential to significantly alter protein properties – could affect additional, so far unknown interactions
355 taking place at this solvent-exposed surface within the complex (**Figure 5G**). To gain insights into whether
356 MCTS1-DENR and MCTS2-DENR could redundantly act in re-initiation, we tested both as recombinant
357 proteins on *Klhdc8a* and *Asb8* reporters. These experiments revealed that both paralogs were able to rescue
358 *Denr* KO extracts in a comparable fashion (**Figure 5H, I**). Taken together, we concluded that *Mcts2*, although
359 previously categorised as a pseudogene [34], is expressed to relevant levels and produces protein that
360 assembles with DENR into protein complexes *in vivo*. *In vitro*, the paralogous complexes show similar activity
361 on our two re-initiation model substrates, indicating redundancy in activity at least for certain substrates.

362 Discussion

363 Translation re-initiation is a process that is at odds with several principles of canonical initiation, termination
364 and post-termination subunit recycling and that remains mechanistically particularly poorly understood. The
365 MCTS1-DENR heterodimer is so far the only reported *trans*-acting factor that is specific to re-initiation, i.e. it
366 does not appear to be essential for general translation as well – quite in contrast to several other proteins that
367 have also been linked to re-initiation in mammals, such as components of eIF3 [13, 35, 36] or eIF4 [13]. For
368 these general eIFs, the analysis of specific re-initiation effects *in vivo*, for example through loss-of-function
369 experiments, is challenging, as they cannot easily be deconvoluted from the abundant global translational
370 alterations and their secondary effects. A defined *in vitro* assay that faithfully recapitulates and quantifies re-
371 initiation gives the possibility of dissecting this process specifically, allowing for targeted, better interpretable
372 experiments. Therefore, we view the development of the *in vitro* re-initiation assay presented in this study as

373 an important methodological advance that will allow the characterisation of *cis*-acting mRNA/uORF sequence
374 requirements and *trans*-acting protein machinery under defined conditions. Our careful benchmarking of the
375 assay, including the use of different reporter constructs and variants, the demonstration of its dependence on
376 MCTS1-DENR using knockout lysates and rescue with recombinant proteins, and the calculation of ribosomal
377 fluxes, demonstrate the suitability of our system for detailed future mechanistic dissection of re-initiation. For
378 example, a strategy to test the requirement for general eIFs in re-initiation could consist in producing HeLa *in*
379 *vitro* translation lysates devoid of the protein of interest (e.g. through acute degron-mediated depletion, just
380 before harvest of the HeLa cells), and to drive uORF translation on the *Klhdc8a* reporter through IRES
381 sequences (e.g. the "factorless" Cricket Paralysis Virus IRES [37]) that bypass the requirement for the
382 particular eIF of interest. Thus, it should be possible to query eIF requirement specifically in re-initiation.
383 Other attractive future applications for our *in vitro* assay include structural biology approaches (i.e., cryo-EM
384 on re-initiation complexes) or compound screens (i.e., testing for specific inhibitors of re-initiation).
385 In addition to the methodological advancement, our study provides important new biological insights, notably
386 regarding MCTS1-DENR and the paralogous MCTS2, as well as on the role that eIF2D plays in gene
387 expression regulation. In particular our observations on eIF2D are surprising, as the *in vivo* and *in vitro*
388 evidence that we provide indicates that the main functions of this protein may not lie in uORF re-initiation
389 after all. In retrospect, the case of eIF2D carrying re-initiation activity in mammals *in vivo* was always heavily
390 built on circumstantial evidence. This evidence was, mainly, the clear homology to MCTS1-DENR, a validated
391 mammalian re-initiation factor; the *in vitro* ability shared by both factors to act on 40S subunits and deliver
392 Met-tRNA$^{Met}_{i}$ to the empty P-site ([14]; using an experimental model where 40S is in complex with HCV
393 IRES-like mRNA); an *in vitro* role of eIF2D for another viral element-dependent translational shuttling
394 phenomenon that resembles re-initiation [38]; the shared *in vitro* activity to promote the release of deacylated
395 tRNA and mRNA from recycled 40S subunits [14]; the high structural similarities of the proteins in
396 reconstituted complexes together with the 40S ribosome [26, 33, 39]; and, finally, *in vivo* evidence in yeast
397 that the orthologous proteins have shared functions which, however, do not lie in uORF re-initiation but in
398 post-termination tRNA removal and 40S ribosome recycling [19] – events from which re-initiation can be
399 envisaged to have subsequently evolved in higher eukaryotes. Finally, two recent studies have observed that
400 eIF2D loss-of-function affected the expression of ATF4 in the integrated stress response in *Drosophila* [22]

401 and of reporter constructs that carried the *Atf4* 5′ UTR (or several other 5′ UTRs containing uORFs) in HeLa
402 cells [21]. These effects were exacerbated by simultaneous DENR loss-of-function, which was interpreted as
403 partially overlapping re-initiation activities of eIF2D and MCTS1-DENR. However, whether the eIF2D-
404 dependent effects indeed relied on the mRNAs' uORFs, or whether they could be mechanistically distinct, was
405 not specifically addressed. Notably, evidence has been accumulating that eIF2D plays roles separate from
406 MCTS1-DENR [20, 28, 40, 41], and the data presented in our study supports this idea as well.
407 Our work, based on the transcriptome-wide analysis of how RNA abundances and translation are altered upon
408 eIF2D depletion, provides evidence that eIF2D is an important regulator of cellular gene expression, as judged
409 from the massive reprogramming at the transcriptome level with hundreds of mRNAs up- and down-regulated
410 and a cell cycle phenotype. However, minor changes occur at the translational level and, moreover, the affected
411 mRNAs are not enriched for uORFs, which points to a main cellular role that does not involve re-initiation
412 and therefore does not overlap with that of MCTS1-DENR. The specific analysis of *Atf4* mRNA in our datasets
413 also supports this model, as we observe increased footprint abundance on the *Atf4* uORF1 stop codon in *Denr*
414 shRNA-treated cells (in line with ribosomal stalling when deacylated tRNA removal is impaired [21]), but not
415 so in *Eif2d* shRNA-treated cells whose profiles are identical to control cells (**Supplementary Figure S6**). Still,
416 since our *in vitro* experiments also reveal that high concentrations of eIF2D can partially compensate for
417 MCTS1-DENR loss, it is quite likely that eIF2D has retained some capacity to act as a re-initiation factor.
418 Whether this activity comes to bear under certain conditions or in specific cell types *in vivo* will require careful
419 further investigations. Probably the most revealing experiment to elucidate the biological function and
420 mechanism by which eIF2D acts, and to distinguish direct from indirect targets in our profiling analyses, would
421 be to identify the mRNAs and sequence elements that eIF2D physically interacts with *in vivo*, for example
422 through selective 40S footprinting [13]. Our efforts in this direction have, unfortunately, not yet been
423 successful.
424 That MCTS2 can act as a *bona fide*, functionally active DENR interaction partner that is expressed to
425 significant levels in the NIH/3T3 cells used for our study, is an important finding as it potentially explains
426 some of the enigmatic published discrepancies between *Mcts1* vs. *Denr* knockout phenotypes. Thus, neuronal
427 migration has been reported to be more strongly perturbed upon DENR loss-of-function than MCTS1 loss-of-
428 function [29]. Moreover, according to the International Mouse Phenotyping Consortium (IMPC;

429 https://www.mousephenotype.org/), *Denr* knockout leads to preweaning lethality with complete penetrance,
430 yet *Mcts1* knockouts are viable, with relatively mild reported phenotypes (mainly affecting eye morphology in
431 early adult animals). The consortium did not phenotype knockouts of *Mcts2*, likely due to its pseudogene
432 assignment. The high *Mcts2* RNA and footprint expression observed in our study could be a particularity of
433 NIH/3T3 cells. Of note, our pilot experiments in mouse embryonic stem cells (mESCs) have recovered MCTS2
434 as an *in vivo* interactor of DENR as well (data not shown), and re-analysis of our previous Ribo-seq data from
435 mouse liver [25] and kidney [42] indicates that MCTS2 is co-expressed alongside MCTS1 in these organs *in*
436 *vivo*, with relative proportions of MCTS1 vs. MCTS2 biosynthesis different across these organs
437 (**Supplementary Figure S7**). Therefore, we propose that MCTS2 is a broadly expressed paralog. In the future,
438 it will be particularly interesting to explore whether MCTS1-DENR and MCTS2-DENR heterodimers have
439 redundant functions or whether the identity of the MCTS paralog has functional consequences for the activity
440 of the heterodimer. Finally, while Bohlen et al. recently reported that *Mcts2* expression is undetectable in
441 various cells of the myeloid lineage (human whole blood cells, THP-1 cells, T-cell blasts) [32], our findings
442 from mouse warrant a more thorough analysis across human tissue and cell types.

443 Material and methods

444 Cloning

445 To generate *in vivo* dual luciferase reporter plasmids, we amplified the 5′ UTRs and first 5 or 10 (depending
446 on construct) CDS codons (in frame with firefly luciferase CDS) of the selected transcripts by PCR from mouse
447 cDNA or genomic DNA and cloned them into the BamHI restriction site of pLV1 dual luciferase reporter
448 plasmid with mutated firefly CDS start, essentially as previously described [17]. Sequences of the primers used
449 for the PCR are reported in Table 1. All constructs were validated by Sanger sequencing.
450 *In vitro* translation reporters were generated by PCR amplification of *Asb8* or *Klhdc8a* 5′ UTRs together with
451 the 6 first CDS codons (in frame with the firefly luciferase CDS, lacking additional ATG start codon), from
452 mouse cDNA, genomic DNA, or the corresponding pLV1 *in vivo* reporter constructs. The PCR products were
453 then cloned into the BamHI restriction site of luciferase T7 control DNA plasmid (Cat. No. L4821, Promega).
454 Modifications of uORFs or other mutations were performed using the Q5 site-directed mutagenesis kit (Cat.

455 No. E0554S, New England Biolabs) and validated by Sanger sequencing. Sequences of primers for PCRs and
456 mutagenesis are reported in Table 2.
457 Plasmids for MCTS1, DENR and eIF2D protein expression have been reported [33] and cloning of human
458 *Mcts2* cDNA for recombinant expression was analogous to that of *Mcts1*; briefly, a fragment encoding the first
459 154 amino acids of MCTS2 (i.e., the part carrying substitutions with regard to MCTS1) was PCR-amplified
460 from HeLa genomic DNA with primers reported in Table 3 and cloned into the XhoI and EcoRV restriction
461 sites of the pLIC C-terminally 6×His-TEV-tagged MCTS1-expression vector [33]. Correct sequence was
462 validated by Sanger sequencing.
463 For endogenous tagging of DENR, a gRNA (GTCATCCACCTAGAAGACACAGG) targeting a downstream
464 sequence of the *Denr* stop codon was inserted into vectors pCas9-2A-mCherry [43] and pRRE200 [44] using
465 oligos described in Table 4.5 µM of oligos were annealed in annealing buffer (100 µM Tris-HCl pH 7.5, 500
466 mM NaCl and 10 mM EDTA) by cooling from 98 °C to 20 °C with a ramp of 0.02 °C per second. Annealed
467 oligos were diluted 10 times then ligated into pCas9-2A-mCherry BsaI restriction site or pRRE200 AatII and
468 SacI restriction sites. Colony PCRs using the reverse gRNA oligo and a pCas9-2A-mCherry or pRRE200
469 forward primer was carried out to check for correct insertion of the annealed oligos and the cloned plasmids
470 validated by Sanger sequencing.
471 A pBluescript II SK(-) vector was ordered as a synthetic clone to contain the knock-in cassette 3×FLAG-
472 NeonGreen-dTAG. *Denr* 5′ and 3′ homology arms were amplified from mouse genomic DNA by PCR using
473 primers reported in Table 4 and ligated in the pBluescript II SK(-) first digested with SpeI and BamHI for the
474 5′ homology arm then with NdeI and KpnI for the 3′ homology arm. Positive clones were identified by colony
475 PCR using PCR homology arm primers and by Sanger sequencing.

476 **Table 1. Sequences of oligonucleotide primers used for the *in vivo* reporters.**

Transcripts	Primer sequences for cloning in prLV1
Klhdc8a	Forward: aaaggatccGTCTCCGACCCTGTAGACACTGCAG
	Reverse: tttggatccactagtATTGGGCACTTCCATGGCAGCCCGG
Klhdc8a start mut	Forward: GGCAGGGAGCCCGTGCAGCGCGgtaccGAGGCTGAGAGAGGGGACGCGCC
	Reverse: GGCGCGTCCCCTCTCTCAGCCTCggtacCGCGCTGCACGGGCTCCCTGCC

Klhdc8a stop mut	Forward: CGGCGCCGTGcacCCCGCGGGCC
	Reverse: GTCGGCGCGTCCCCTCTCTC
Med23	Forward: aaaggatccAGAGCAAGAGAGAGCGGCG
	Reverse: tttggatccactagtGCTCTGCAGTTGCGTCTCCATC
Rps20	Forward: aaaggatccGTTCCGGGTCACAAAGCACC
	Reverse: tttggatccactagtGGGCGTCTTTCCGGTATCTTTAAATG
Cenpa	Forward: aaaggatccATTGGCTTCAGACCTTTATTCTCATTGG
	Reverse: tttggatccactagtTGGGGTCTGCGGTTTGCGAC
Ndc80	Forward: aaaggatccTGACGTCAGCGCGGGCG
	Reverse: tttggatccactagtACCACAGGTGGAAACTGAACTGCG

477 **Table 2. Sequences of oligonucleotide primers used for the *in vitro* reporters.**

Transcripts	Primer sequences for cloning in pT7luc
Klhdc8a start mut	Forward: ggtGAAGACGCCAAAAACATAAAG
	Reverse: ttgaATCCTGACATTGGGCACT
Klhdc8a stop mut	Forward: CGGCGCCGTGcacCCCGCGGGCC
	Reverse: GTCGGCGCGTCCCCTCTCTC
Klhdc8a deletion 499bp 5′ UTR	Forward: GGTGTCAGCGGGGCAGCAAGCTTGGGAGGCCTTA
	Reverse: TAAGGCCTCCCAAGCTTGCTGCCCCGCTGACACC
Klhdc8a penultimate codon GTC (WT & start mut)	Forward: GACCGGCGCCGTCTAGCCCGCGG
	Reverse: GGCGCG TCCCCTCTCTCAGC
Klhdc8a penultimate codon GTC (stop mut)	Forward: GACCGGCGCCGTCCACCCCGCGG
	Reverse: GGCGCGTCCCCTCTCTCAGCCTCC
Klhdc8a penultimate codon GCG (WT & start mut)	Forward: GACCGGCGCCGCGTAGCCCGCGG
	Reverse: GGCGCGTCCCCTCTCTCAGCC

Klhdc8a penultimate codon GCG (stop mut)	Forward: GACCGGCGCCGCGCACCCCGCGG
	Reverse: GGCGCGTCCCCTCTCTCAGCCTCC
Asb8	Forward: aaaggatccTTCTGCTTCCGGGTCACGCC
	Reverse: tttggatcctCCACATGCTGGAACTCATCAAGG
Asb8 start mut	Forward: CGTTTGGAGCaccTGAACACACTCTGAGCCTTGATGAG
	Reverse: AACCGCGGGTCAGATCGG

478 **Table 3. Sequences of oligonucleotide primers used for cloning the pLIC C-terminally 6x-His-TEV-**
479 **tagged *Mcts2* vector.**

Transcripts	Primer sequences for cloning in pLIC
hsMcts2	Forward: AAACTCGAGTTCTAGAAATAATTTTGTTTAACTTTAAGAAGGAGATATAGATCATGTTCAAGAAGTTTGATGAAAAGG
	Reverse: AAAGATATCTTCTGCAGACATCTTCATGAC

480 **Table 4. Sequences of oligonucleotides used for the cloning of *Denr* gRNA and homology arms into the**
481 **pCas9-2A-mCherry, pRRE200 and pBluescript II SK(-).**

Plasmids	Primers type	Oligo sequences
pCas9-2A-mCherry	Annealing oligos	Forward: caccgGTCATCCACCTAGAAGACAC
		Reverse: aaacGTGTCTTCTAGGTGGATGACc
	Colony PCR	Forward: GCCTATTTCCCATGATTCCTTCA
pRRE200	annealing oligos	Forward: GTCGTCATCCACCTAGAAGACACAGGTGAACGT
		Reverse: aaacGTGTCTTCTAGGTGGATGACc
	Colony PCR	Forward: CCACTTTGCCTTTCTCTCCACAG
pBluescript II SK(-)	To PCR 5′ homology arm	Forward: aaaactagtATTTAAAATGTAGATGAAATTTCAAAATGAAG
		Reverse: aaaggatccCTTCTTCACTTCTCCAAGG
	To PCR 3′	Forward: aaaattaatTGATCCTGAAGTCATGTGTTTCTAACTG

	homology arm	Reverse: aaaggtaccTGCACGAGGCCCTGGGTTC
	Q5 mutagenesis	Forward: GTTCTTTCACgTGTGTCTTCTAG
		Reverse: TTCATGAATTGTGGCCAAAAC

482 **Cell culture and generation of HeLa knockout cells**

483 NIH/3T3, HEK293FT and HeLa cells were cultured under standard conditions (DMEM; 10 % FCS, 1 %
484 penicillin/streptomycin, all from Invitrogen; 37 °C; 5 % CO_2). The HeLa *Denr* knockout (KO) cells have been
485 published [21]. For *Eif2d* KOs, wild-type HeLa cells were seeded in a 6-well plate (200,000 cells per well) in
486 DMEM with 10 % FBS and 1 % Pen/Strep. After 24 h the cells were transfected with plasmid pX459 v2.0 into
487 which an sgRNA sequence targeting *Eif2d* was cloned (sequence: CACCGCTGTGGACTGGAAACACCCG)
488 using Lipofectamine 2000 following the manufacturer's instructions. 24 h later, lipofectamine was removed
489 and cells were kept in DMEM for recovery for 2 days. On the third day, puromycin was added to a final
490 concentration of 1.5 µg/ml. After another 3 days, puromycin was removed and fresh medium was added. After
491 2 days, cells were seeded into a 96-well plate at limiting dilution, so that only one cell per well was seeded.
492 Wells were checked under the microscope for single cell colonies. Upon reaching confluency wells with only
493 one colony were reseeded into 6-well plate and kept for growing. Then immunoblots on these monoclonal lines
494 were performed to identify the ones with loss of eIF2D. The knockout was verified at the genomic level via
495 PCR using the following primers: 5′-GGGGAGGGCTCGGGTATGAC-3′ and 5′-
496 AAGGCAGGGGCTGTCTCATATC-3′ to amplify the genomic region. This revealed premature stop codons
497 in all alleles. For generating *Eif2d / Denr* double knockout cells, the same procedure was performed to
498 introduce the *Eif2d* knockout into the previously published *Denr*-knockout HeLa line [21].

499 **Lentiviral transduction**

500 Lentiviral shRNA plasmids targeting *Eif2d* were purchased from Sigma (Cat. No. TRCN0000119842 for non-
501 functional (nf) shRNA, TRCN0000119844 for shRNA1 and TRCN0000119845 for shRNA2). The *Denr*
502 ("*Denr* shRNA2") and Scramble shRNA plasmids have been described previously [17]. Production of
503 lentiviral particles in HEK293FT cells using envelope pMD2.G and packaging psPAX2 plasmids and viral
504 transduction of NIH/3T3 cells were performed following published protocols [17, 45], with puromycin
505 selection at 5 µg/ml for 4 days for shRNA transduced cells.

506 **Western Blot**

507 Total protein extracts from NIH/3T3 and HeLa cells were prepared according to the NUN method [46]. For
508 analysis of phosphorylated proteins, PhosSTOP™ (Cat. No. 4906845001, Roche) was included in the NUN
509 buffer. Antibodies used were rabbit anti-KLHDC8A 1:5000 (ab235419, Abcam), rabbit anti-VINCULIN
510 1:5000 (ab129002, Abcam) mouse anti-U2AF65 1:5000 (U4758, Sigma), rabbit anti-EIF2D 1:750 (12840-1-
511 AP, Proteintech), rabbit anti-DENR 1:5000 (ab108221, Abcam), rabbit anti-phospho-eIF2alpha (Ser51) 1:1000
512 (#9721S, Cell Signaling), mouse anti-FLAG 1:10000 (M2F3165, Sigma), rabbit anti-RPL23 (ab112587,
513 Abcam), mouse anti-beta-Tubulin 1:5000 (T5201, Sigma) and secondaries goat anti-guinea pig-HRP 1:10000
514 (SA00001-12, Proteintech), anti-rabbit-HRP (W4011, Promega) and anti-mouse-HRP 1:10000 (S3721,
515 Promega). The guinea-pig anti-MCTS1 antibodies (used at 1:500) have been described (Schleich et al. 2014).
516 Blots were visualized with the Fusion Fx7 system.

517 **Translation-competent extract preparation**

518 The overall protocol for extract preparation was an adaptation of that published by Gurzeler et al., 2022 [23].
519 Briefly, confluent 15-cm dishes of HeLa cells were washed once with PBS at 37 °C, then trypsinized with
520 0.05 % Trypsin-EDTA (Cat. No. 25300054, Gibco™). Harvested cells were collected by centrifugation at 500
521 × *g* for 5 min at 4 °C. The cell pellet was washed twice with ice-cold PBS and centrifugation at 200 × *g* for 5
522 min at 4 °C. The cell pellet was resuspended in 1:1 lysis buffer (10 mM HEPES pH 7.3, 10 mM potassium
523 acetate, 500 µM $MgCl_2$, 5 mM DTT and 1× cOmplete™ EDTA-free Protease Inhibitor Cocktail (Cat. No.
524 4693132001, Roche)). Cells were lysed by dual centrifugation at 500 RPM for 4 min at −5 °C using a
525 ZentriMix 380 R centrifuge (Hettich AG) with a 3206 rotor and 3209 adapters. The resulting lysate was then
526 centrifuged in a table-top centrifuge at 13,000 × *g* at 4 °C for 10 min and the supernatant was aliquoted and
527 snap-frozen in liquid nitrogen; storage at −80 °C for up to 6 months.

528 **Expression and purification of recombinant proteins**

529 Recombinant EIF2D, MCTS1 and DENR protein purification has been described [33]. Recombinant MCTS2
530 was expressed and purified identically to MCTS1. GADD34Δ1-240 expression plasmid has been described
531 [23]; for protein preparation, bacterial strain BL-21 (DE-3) (pLysS) was transformed with the plasmid, grown
532 in 1000 ml Luria broth at 37 °C until the OD600 reached 0.4–0.6. After induction (1 mM IPTG) bacteria were
533 cultured for another 4 h and cells were harvested. Expression of recombinant GADD34Δ1-240 was validated

534 on Coomassie gel. The cell pellet was resuspended in 50 ml lysis/wash buffer (50 mM Tris-HCl pH 7.5, 300
535 mM NaCl, 5 % glycerol, 25 mM imidazole), lysed by sonication with 240 × 1 s pulses at 40 % amplitude on
536 ice and centrifuged at 18,000 × *g* for 20 min at 4 °C. The supernatant was mixed with 1 ml HisPur Ni-NTA
537 washed resin slurry (Cat. No. 88222, Thermo Fisher Scientific) for at least 2 h at 4 °C under continuous
538 rotation. Unbound proteins and background were removed by washing the resin 2× with 50 ml of lysis/wash
539 buffer, then bound proteins were eluted 2× with 3 ml elution buffer (lysis/wash buffer supplemented with 400
540 mM imidazole). The proteins were dialyzed in protein reconstitution buffer (30 mM NaCl, 5 mM HEPES pH
541 7.3) overnight using a Slide-A-Lyzer Dialysis Cassette (MWCO 10K) (Cat. No. 88400TS, Thermo Fisher
542 Scientific) at 4 °C under agitation. Protein concentration was quantified with a nanodrop device.

543 ***In vitro* transcription**

544 Reporter DNA templates were PCR-amplified before transcription for 2 h using the MEGAscript® T7
545 Transcription Kit protocol (AM1334, Invitrogen) (forward primer: GCGCGTTGGCCGATTCATTAATGC;
546 reverse primer: T_{100}GGGAGCTCGCCCCCTCGGAG). Capping was carried out co-transcriptionally using the
547 CleanCap Reagent AG (3′ Ome) (N-7413, TriLink) and the Yeast Inorganic Pyrophosphatase (Cat. No.
548 M2403S, New England BioLabs) following the CleanCap protocol. The capped RNAs were treated for 15 min
549 at 37 °C with 0.14 U/µl Turbo DNase (AM2238, Invitrogen), then purified using the Monarch RNA Cleanup
550 Kit (T2040L, New England Biolabs). Quality and size of the produced RNAs were assessed using an Agilent
551 Fragment Analyzer.

552 ***In vitro* translation assay**

553 6.5 µl of translation-competent extracts were freshly supplemented with 0.4 mM amino acids (L4461,
554 Promega), 15 mM HEPES pH 7.3, 6 mM Creatine Phosphate, 102 ng/ml Creatine kinase, 28 mM potassium
555 acetate, 1 mM $MgCl_2$, 24 mM KCl, 1 U/µl RNasin® Plus Ribonuclease Inhibitor (N2611, Promega) and 2
556 fmol/µl of Renilla luciferase reporter in a final volume of 12.5 µl prior to each *in vitro* translation assay. Unless
557 specified, 16 ng/µl of recombinant GADD34Δ1-240 was included to the supplemented extracts. 30 fmol/µl of
558 firefly luciferase reporter were used per reaction. The *in vitro* translation assays were carried out at 37 °C for
559 50 min. Luminescence activity was quantified using the Dual-Glo® Luciferase Assay System (E2940,
560 Promega) and a Tecan Safire2™ plate reader.

561 ***In vivo* dual luciferase assay**

562 NIH/3T3 cells were first stably transduced with the lentiviral dual luciferase reporters containing the 5′ UTRs
563 to be assayed (upstream of firefly luciferase) and Renilla luciferase (internal normalisation), bidirectionally
564 driven by the *Pgk1* promoter. After establishing the reporter-expressing cell population and several passages
565 to ensure stable expression, cells were transduced with the shRNA lentiviruses and selected on puromycin for
566 4 days before lysis in 1× passive lysis buffer (E1941, Promega) and dual luciferase readout using the Dual-
567 Glo® Luciferase Assay System (E2940, Promega) and a Tecan Safire2™ plate reader.

568 **Ribosome profiling and library preparation**

569 One 15-centimeter dish of confluent NIH/3T3 cells was used per replicate. Ribosome profiling and parallel
570 RNA-seq were performed in triplicate for *Denr* shRNA2, *Eif2d* shRNA1, *Eif2d* shRNA2, non-functional (nf)
571 *Eif2d* shRNA and Scr shRNA transduced cells, closely following our previously reported protocol [17] with
572 minor modifications as described below. Cells were washed in cold PBS (without cycloheximide), harvested
573 by scraping down in small volume of PBS (without cycloheximide), pelleted by brief centrifugation, then flash
574 frozen. Cell lysates were prepared as described (with cycloheximide) [17]. For the generation of ribosome-
575 protected fragments, cell lysates were treated with 5 units RNaseI (ART-Seq, Epicenter/Illumina) per OD260,
576 and monosomes were purified on MicroSpin S-400 columns (GE Healthcare). For both Ribo- and RNA-seq,
577 2 µg of RNA was used for rRNA depletion following the RiboCop rRNA Depletion Kit V1.2 (Cat. No. 037.24,
578 Lexogen). Finally, libraries were amplified using 10-14 PCR cycles, and sequenced (HiSeq2500 platform).

579 **Sequencing pre-processing, alignment, quantification**

580 Sequencing reads were processed as described previously [47]. Briefly, sequencing adapters were trimmed
581 using Cutadapt [48] and the reads were size filtered by a custom Python script (26-35 nt for RPF and 21-60 nt
582 for RNA). The reads were then aligned subsequently to mouse rRNA, human rRNA, mouse tRNA and mouse
583 cDNA from Ensembl mouse database release 100 using Bowtie2 [49]. In order to estimate expressed isoforms,
584 the RNA-seq reads were mapped in parallel to the mouse genome using STARmapper version 2.5.3a [50] and
585 processed with StringTie [51] to measure FPKM for each transcript. A custom Python script classified the
586 transcripts into single expressed isoform or multiple transcript isoforms. The mapped reads were counted on
587 5′ UTR or CDS of the protein coding genes using a custom Python script. The location of the putative A-site
588 of RPFs were estimated as 5′ position +16 for reads shorter than or equal to 31 nt and +17 for reads longer
589 than 31 nt. Transcripts for which there were less than 10 counts in total of all samples were filtered out of the

590 further analysis. Read counts were normalized using the upper quartile normalization method [52] from edgeR
591 [52] then transformed to transcripts per million (TPM) to normalize for transcript length. Translation
592 efficiencies were calculated as the $\log_2$-transformed ratio of normalized CDS footprint counts to normalized
593 CDS RNA counts and averaged over replicates. All analyses were carried out on R version 4.2.1.

594 **Differential translation efficiency analysis**

595 Ribosome profiling sequencing data were analysed using the deltaTE method [53] in order to assess significant
596 changes in translation efficiency and RNA abundance. Significance threshold was set to FDR < 0.1.

597 **uORF annotation and analyses**

598 For uORF annotation, transcripts were used for which reads could be unambiguously assigned to the 5′ UTR,
599 i.e. transcripts that are the only protein-coding isoform expressed (single expressed isoform) (N = 6841). In
600 order to include as many transcripts as possible for the annotations, genes with multiple protein coding
601 isoforms were also considered if all expressed isoforms had the same CDS start, in which case the transcript
602 with the longest 5′ UTR was selected (N = 2425). For the selected transcripts, uORFs were annotated and
603 considered as translated with the following criteria: (i) they started with AUG, CUG, GUG or UUG, (ii) they
604 had an in-frame stop codon within the 5′ UTR, and (iii) they had a coverage of at least 33 %. When several
605 potential uORFs were overlapping, the one with the highest coverage (read count/uORF length) was
606 considered.

607 **Cell cycle monitoring**

608 The cell proliferation assay was performed using the Click-iT® EdU Flow Cytometry Assay Kits (C10424,
609 Invitrogen) following the vendor's protocol with some modifications. Briefly, NIH/3T3 cells transduced with
610 scramble shRNA, nf *Eif2d* shRNA, *Denr* shRNA and *Eif2d* shRNA1 and shRNA2 were seeded into 6-cm
611 plates under puromycin selection. After 4 days, the cells were treated for 1 h with 10 µM of EdU, washed with
612 PBS, trypsinized and collected into FACS tubes. The cells were then centrifuged at 1200 × *g* for 5 min and
613 resuspended in PBS. The cells were counted, and all conditions were adjusted to the same number of cells.
614 After washing with 3 ml of 1 % BSA in PBS, the cells were resuspended in 100 µl fixative buffer and incubated
615 overnight at 4 °C. Another wash with 1 % BSA in PBS followed by a 15 min incubation in 100 µl of 1×-
616 saponin-based permeabilization and wash reagent. 200 µl of Click-iT reaction cocktail were added to each tube
617 and the cells were incubated for 30min at room temperature. After a wash in 3 ml of 1 % BSA in PBS, the cells

618 were resuspended in 100 µl of 1×-saponin-based permeabilization and wash reagent complemented with 5µl
619 of 20 mg/ml RNaseA and 2 µl of 1 mg/ml propidium iodide and incubated for 30 min at room temperature.
620 Fluorescence was measured using Accuri C6 FACS machine.

621 **Generation of endogenously tagged cell lines**

622 C-terminal tagging of endogenous DENR with 3×FLAG-NeonGreen-dTAG in NIH/3T3 cells was carried out
623 using CRISPR-Cas9 homology-directed repair. 10^5 NIH/3T3 cells were seeded in a 6-well plate 24h prior to
624 transfection. 0.9 µg of the pBLU donor plasmid (containing 400 bp 5′ and 3′ homology arms directly upstream
625 and downstream of *Denr* stop codon) as well as 0.5 µg of the pCas9-gRNA and 0.1 µg of the control pRRE
626 reporter were transfected into NIH/3T3 using Lipofectamine™ 3000 (L3000008, Invitrogen). Medium was
627 changed after 24 h and cells were FACS sorted based on mCherry and EGPF expression in a 10 cm dish 48 h
628 post-transfection. Cells were counted and diluted to have 1 cell per well of a 96-well plate. When cell clones
629 became visible, they were preselected based on NeonGreen expression, then split into a 96-well plate for
630 genotyping and a 12-well plate for maintenance. For genomic DNA extraction, cells were washed with PBS
631 then lysed in 20 µl of DNA lysis buffer (10 mM Tris-HCl pH 8, 0.5 mM EDTA, 0.5 % Triton X-100, 0.5 mg/ml
632 proteinase K). After incubation for 1 h at 55 °C, cooling on ice and further incubation for 10 min at 95 °C to
633 inactivate proteinase K, this prep was used to check the insertion of the cassette into the *Denr* locus by PCR
634 using primers upstream of the 5′ and downstream of the 3′ homology arms.

635 **Co-immunoprecipitation**

636 Triplicate 15 cm plates of 80 % confluent NIH/3T3 DENR-3×FLAG-NeonGreen-dTAG cells were treated with
637 500 nM dTAG-13 or control-treated for 5 h prior to harvesting. After washing with PBS, cells were scraped in
638 1 ml PBS (4 °C). Cells were collected by centrifugation at 500 × *g* for 5min at 4 °C and lysed in 400 µl IP
639 buffer (50 mM Tris-HCl pH 7.5, 120 mM NaCl, 1 % NP-40, 0.5 mM DTT, 10 mM $MgCl_2$, 1× PhosSTOP™
640 (4906837001, Roche), 1× cOmplete™ EDTA-free Protease Inhibitor Cocktail (Cat. No. 4693132001, Roche),
641 0.04 U/µl RNasin® Plus Ribonuclease Inhibitor (CN2611, Promega)) for 30 min on ice with mixing by
642 pipetting every 10 min. Lysed cells were centrifuged for 7 min at 5000 × *g* at 4 °C and the supernatant was
643 collected. Proteins were quantified using Pierce™ BCA Protein Assay kit (Cat. No. 23225, Thermo Fisher
644 Scientific) and 500 µl of 2 mg/ml proteins were incubated with washed anti-FLAG magnetic beads (Cat. No.
645 M8823, Millipore) at 4 °C for 3 h on rotating wheel. The flow-through was kept for Western Blot and beads

646 were washed twice in wash buffer (20 mM Tris-HCl pH 7.5, 100 mM NaCl, 0.5 mM DTT, 10 mM $MgCl_2$, 1×
647 cOmplete™ EDTA-free Protease Inhibitor Cocktail (Cat. No. 4693132001, Roche), 0.04 U/µl RNasin® Plus
648 Ribonuclease Inhibitor (N2611, Promega)) with change of tubes between the 1st and the 2nd wash. Proteins
649 were eluted in 80 µl elution buffer (NH_4OH pH 11-12) and incubated for 15 min at 4 °C. Elution step was
650 repeated twice and eluates were pooled, frozen and dried in a SpeedVac system.

651 **Mass-spectrometry and data analysis**

652 Samples were digested following a modified version of the iST method (named miST method). Briefly, dried
653 material was redissolved in 50 µl miST lysis buffer (1 % Sodium deoxycholate, 100 mM Tris pH 8.6, 10 mM
654 DTT), heated 5 min at 95 °C and diluted 1:1 (v:v) with water. Reduced disulfides were alkylated by adding ¼
655 vol. of 16 0mM chloroacetamide (32 mM final) and incubating for 45 min at RT in the dark. Samples were
656 adjusted to 3 mM EDTA and digested with 1.0 µg Trypsin/LysC mix (Promega #V5073) for 1 h at 37 °C,
657 followed by a second 1 h digestion with an additional 0.5 µg of proteases. To remove sodium deoxycholate,
658 two sample volumes of isopropanol containing 1 % TFA were added to the digests, and the samples were
659 desalted on a strong cation exchange (SCX) plate (Oasis MCX; Waters Corp., Milford, MA) by centrifugation.
660 After washing with isopropanol/1 % TFA, peptides were eluted in 200 µl of 80 % MeCN, 19 % water, 1 %
661 (v/v) ammonia, and dried by centrifugal evaporation. Tryptic peptide mixtures were injected on an Ultimate
662 RSLC 3000 nanoHPLC system interfaced via a nanospray Flex source to a high resolution Orbitrap Exploris
663 480 mass spectrometer (Thermo Fisher, Bremen, Germany). Peptides were loaded onto a trapping
664 microcolumn Acclaim PepMap100 C18 (20 mm × 100 µm ID, 5 µm, Dionex) before separation on a C18
665 custom packed column (75 µm ID × 45 cm, 1.8 µm particles, Reprosil Pur, Dr. Maisch), using a gradient from
666 4 % to 90 % acetonitrile in 0.1 % formic acid for peptide separation (total time: 140 min). Full MS survey
667 scans were performed at 120,000 resolution. A data-dependent acquisition method controlled by Xcalibur
668 software (Thermo Fisher Scientific) was used that optimised the number of precursors selected ("top speed")
669 of charge 2+ to 5+ while maintaining a fixed scan cycle of 2 s. Peptides were fragmented by higher energy
670 collision dissociation (HCD) with a normalized energy of 30 % at 15,000 resolution. The window for precursor
671 isolation was of 1.6 *m/z* units around the precursor and selected fragments were excluded for 60s from further
672 analysis. Data files were analysed with MaxQuant 1.6.14.0 incorporating the Andromeda search engine
673 Cysteine carbamidomethylation was selected as fixed modification while methionine oxidation and protein N-

674 terminal acetylation were specified as variable modifications. The sequence databases used for searching were
675 the mouse *(Mus musculus)* reference proteome based on the UniProt database (www.uniprot.org, version of
676 April 6th, 2021, containing 55,341 sequences RefProt _Mus_musculus_20210604.fasta) supplemented with the
677 sequences of common contaminants, and a database of mammalian immunoglobulin sequences
678 (https://www.imgt.org version of 20th Nov. 2018, 2243 entries). Mass tolerance was 4.5 ppm on precursors
679 (after recalibration) and 20 ppm on MS/MS fragments. Both peptide and protein identifications were filtered
680 at 1 % FDR relative to hits against a decoy database built by reversing protein sequences. All subsequent
681 analyses were done with the Perseus software package (version 1.6.15.0). Contaminant proteins were removed,
682 and intensity iBAQ values were $\log_2$-transformed. After assignment to groups, only proteins quantified in at
683 least 3 samples of one group were kept. After missing values imputation (based on normal distribution using
684 Perseus default parameters), *t*-tests were carried out among all conditions, with permutation-based FDR
685 correction for multiple testing (Q-value threshold < 0.05). Log_2FC of non-treated Denr-3×FLAG-NeonGreen-
686 dTAG vs. dTAG treated Denr-3×FLAG-NeonGreen-dTAG was calculated and p-value was corrected for
687 multiple testing by False discovery rate (significance threshold was set to FDR < 0.05).

688 **Acknowledgements**

689 We thank the Lausanne Genomic Technologies Facility for library sequencing and the Lausanne Protein
690 Analysis Facility for mass spectrometry-based proteomics. Evan Karousis for help with the initial setup of the
691 *in vitro* translation assay and for the GADD34Δ1-240-expression plasmid, and Michael Taschner for his help
692 with preparation of recombinant GADD34Δ1-240. We thank members of the Gatfield lab for critical comments
693 on the manuscript.

694 **Funding**

695 This work was supported by Swiss National Science Foundation (SNSF) NCCR RNA & Disease Phase III
696 funding, grant number 205601 (to D.G. and N.B.) and by SNSF Project funding, grant number 212423 (to
697 D.G.).

698 **Author contributions**

699 Conceptualization: D.G., R.M. Methodology: R.M., M.D.M., A.B., T.W. Investigation: R.M., M.D.M., N.G.
700 Visualization: R.M., N.G., A.B., D.G. Supervision: D.G., N.B., A.A.T. Writing original draft: R.M., D.G.

701 **Competing interests**

The authors declare that they have no competing interests.

Data and script availability

Sequencing data have been deposited at GEO (GSE263991) with reviewer token: *(see cover letter)* and mass spectrometry data at PRIDE (PXD051482), with username: reviewer_pxd051482@ebi.ac.uk and password: *(see cover letter)*.

References

1. Wethmar K: **The regulatory potential of upstream open reading frames in eukaryotic gene expression.** *Wiley Interdiscip Rev RNA* 2014, **5:**765-778.
2. Jousse C, Bruhat A, Carraro V, Urano F, Ferrara M, Ron D, Fafournoux P: **Inhibition of CHOP translation by a peptide encoded by an open reading frame localized in the chop 5'UTR.** *Nucleic Acids Res* 2001, **29:**4341-4351.
3. Lee YY, Cevallos RC, Jan E: **An upstream open reading frame regulates translation of GADD34 during cellular stresses that induce eIF2alpha phosphorylation.** *J Biol Chem* 2009, **284:**6661-6673.
4. Hinnebusch AG, Ivanov IP, Sonenberg N: **Translational control by 5'-untranslated regions of eukaryotic mRNAs.** *Science* 2016, **352:**1413-1416.
5. Clemm von Hohenberg K, Müller S, Schleich S, Meister M, Bohlen J, Hofmann TG, Teleman AA: **Cyclin B/CDK1 and Cyclin A/CDK2 phosphorylate DENR to promote mitotic protein translation and faithful cell division.** *Nat Commun* 2022, **13:**668.
6. Schulz J, Mah N, Neuenschwander M, Kischka T, Ratei R, Schlag PM, Castaños-Vélez E, Fichtner I, Tunn PU, Denkert C, et al: **Loss-of-function uORF mutations in human malignancies.** *Sci Rep* 2018, **8:**2395.
7. Occhi G, Regazzo D, Trivellin G, Boaretto F, Ciato D, Bobisse S, Ferasin S, Cetani F, Pardi E, Korbonits M, et al: **A novel mutation in the upstream open reading frame of the CDKN1B gene causes a MEN4 phenotype.** *PLoS Genet* 2013, **9:**e1003350.
8. von Bohlen AE, Böhm J, Pop R, Johnson DS, Tolmie J, Stücker R, Morris-Rosendahl D, Scherer G: **A mutation creating an upstream initiation codon in the SOX9 5' UTR causes acampomelic campomelic dysplasia.** *Mol Genet Genomic Med* 2017, **5:**261-268.
9. Hornig NC, de Beaufort C, Denzer F, Cools M, Wabitsch M, Ukat M, Kulle AE, Schweikert HU, Werner R, Hiort O, et al: **A Recurrent Germline Mutation in the 5'UTR of the Androgen Receptor Causes Complete Androgen Insensitivity by Activating Aberrant uORF Translation.** *PLoS One* 2016, **11:**e0154158.
10. Schleich S, Strassburger K, Janiesch PC, Koledachkina T, Miller KK, Haneke K, Cheng YS, Kuchler K, Stoecklin G, Duncan KE, Teleman AA: **DENR-MCT-1 promotes translation re-initiation downstream of uORFs to control tissue growth.** *Nature* 2014, **512:**208-212.
11. Schleich S, Acevedo JM, Clemm von Hohenberg K, Teleman AA: **Identification of transcripts with short stuORFs as targets for DENR•MCTS1-dependent translation in human cells.** *Sci Rep* 2017, **7:**3722.
12. Mohammad MP, Munzarova Pondelícková V, Zeman J, Gunišová S, Valášek LS: **In vivo evidence that eIF3 stays bound to ribosomes elongating and terminating on short upstream ORFs to promote reinitiation.** *Nucleic Acids Res* 2017, **45:**2658-2674.
13. Bohlen J, Fenzl K, Kramer G, Bukau B, Teleman AA: **Selective 40S Footprinting Reveals Cap-Tethered Ribosome Scanning in Human Cells.** *Mol Cell* 2020, **79:**561-574.
14. Skabkin MA, Skabkina OV, Dhote V, Komar AA, Hellen CU, Pestova TV: **Activities of Ligatin and MCT-1/DENR in eukaryotic translation initiation and ribosomal recycling.** *Genes Dev* 2010, **24:**1787-1801.
15. Skabkin MA, Skabkina OV, Hellen CU, Pestova TV: **Reinitiation and other unconventional posttermination events during eukaryotic translation.** *Mol Cell* 2013, **51:**249-264.

16. Zlotorynski E: **Translation. DENR-MCT1 reinitiates translation.** *Nat Rev Mol Cell Biol* 2014, **15:**498.
17. Castelo-Szekely V, De Matos M, Tusup M, Pascolo S, Ule J, Gatfield D: **Charting DENR-dependent translation reinitiation uncovers predictive uORF features and links to circadian timekeeping via Clock.** *Nucleic Acids Res* 2019, **47:**5193-5209.
18. Dmitriev SE, Terenin IM, Andreev DE, Ivanov PA, Dunaevsky JE, Merrick WC, Shatsky IN: **GTP-independent tRNA delivery to the ribosomal P-site by a novel eukaryotic translation factor.** *J Biol Chem* 2010, **285:**26779-26787.
19. Young DJ, Makeeva DS, Zhang F, Anisimova AS, Stolboushkina EA, Ghobakhlou F, Shatsky IN, Dmitriev SE, Hinnebusch AG, Guydosh NR: **Tma64/eIF2D, Tma20/MCT-1, and Tma22/DENR Recycle Post-termination 40S Subunits In Vivo.** *Mol Cell* 2018, **71:**761-774.
20. Young DJ, Meydan S, Guydosh NR: **40S ribosome profiling reveals distinct roles for Tma20/Tma22 (MCT-1/DENR) and Tma64 (eIF2D) in 40S subunit recycling.** *Nat Commun* 2021, **12:**2976.
21. Bohlen J, Harbrecht L, Blanco S, Clemm von Hohenberg K, Fenzl K, Kramer G, Bukau B, Teleman AA: **DENR promotes translation reinitiation via ribosome recycling to drive expression of oncogenes including ATF4.** *Nat Commun* 2020, **11:**4676.
22. Vasudevan D, Neuman SD, Yang A, Lough L, Brown B, Bashirullah A, Cardozo T, Ryoo HD: **Translational induction of ATF4 during integrated stress response requires noncanonical initiation factors eIF2D and DENR.** *Nat Commun* 2020, **11:**4677.
23. Gurzeler LA, Ziegelmüller J, Mühlemann O, Karousis ED: **Production of human translation-competent lysates using dual centrifugation.** *RNA Biol* 2022, **19:**78-88.
24. Mikami S, Kobayashi T, Imataka H: **Cell-free protein synthesis systems with extracts from cultured human cells.** *Methods Mol Biol* 2010, **607:**43-52.
25. Janich P, Arpat AB, Castelo-Szekely V, Lopes M, Gatfield D: **Ribosome profiling reveals the rhythmic liver translatome and circadian clock regulation by upstream open reading frames.** *Genome Res* 2015, **25:**1848-1859.
26. Ahmed YL, Schleich S, Bohlen J, Mandel N, Simon B, Sinning I, Teleman AA: **DENR-MCTS1 heterodimerization and tRNA recruitment are required for translation reinitiation.** *PLoS Biol* 2018, **16:**e2005160.
27. Dever TE, Ivanov IP, Hinnebusch AG: **Translational regulation by uORFs and start codon selection stringency.** *Genes Dev* 2023, **37:**474-489.
28. Alghoul F, Laure S, Eriani G, Martin F: **Translation inhibitory elements from Hoxa3 and Hoxa11 mRNAs use uORFs for translation inhibition.** *Elife* 2021, **10:**e66369.
29. Haas MA, Ngo L, Li SS, Schleich S, Qu Z, Vanyai HK, Cullen HD, Cardona-Alberich A, Gladwyn-Ng IE, Pagnamenta AT, et al: **De Novo Mutations in DENR Disrupt Neuronal Development and Link Congenital Neurological Disorders to Faulty mRNA Translation Re-initiation.** *Cell Rep* 2016, **15:**2251-2265.
30. Nabet B, Roberts JM, Buckley DL, Paulk J, Dastjerdi S, Yang A, Leggett AL, Erb MA, Lawlor MA, Souza A, et al: **The dTAG system for immediate and target-specific protein degradation.** *Nat Chem Biol* 2018, **14:**431-441.
31. Wood AJ, Roberts RG, Monk D, Moore GE, Schulz R, Oakey RJ: **A screen for retrotransposed imprinted genes reveals an association between X chromosome homology and maternal germ-line methylation.** *PLoS Genet* 2007, **3:**e20.
32. Bohlen J, Zhou Q, Philippot Q, Ogishi M, Rinchai D, Nieminen T, Seyedpour S, Parvaneh N, Rezaei N, Yazdanpanah N, et al: **Human MCTS1-dependent translation of JAK2 is essential for IFN-gamma immunity to mycobacteria.** *Cell* 2023, **186:**5114-5134.
33. Weisser M, Schäfer T, Leibundgut M, Böhringer D, Aylett CHS, Ban N: **Structural and Functional Insights into Human Re-initiation Complexes.** *Mol Cell* 2017, **67:**447-456vala.
34. Nandi S, Shi B, Perreault J, Gartenhaus RB: **Characterization of the MCT-1 pseudogene: identification and implication of its location in a highly amplified region of chromosome 20.** *Biochim Biophys Acta* 2006, **1759:**234-239.
35. Hronová V, Mohammad MP, Wagner S, Pánek J, Gunišová S, Zeman J, Poncová K, Valášek LS: **Does eIF3 promote reinitiation after translation of short upstream ORFs also in mammalian cells?** *RNA Biol* 2017, **14:**1660-1667.

806 36. Shu XE, Mao Y, Jia L, Qian SB: **Dynamic eIF3a O-GlcNAcylation controls translation**
807 **reinitiation during nutrient stress.** *Nat Chem Biol* 2022, **18:**134-141.
808 37. Pestova TV, Hellen CU: **Translation elongation after assembly of ribosomes on the**
809 **Cricket paralysis virus internal ribosomal entry site without initiation factors or**
810 **initiator tRNA.** *Genes Dev* 2003, **17:**181-186.
811 38. Zinoviev A, Hellen CUT, Pestova TV: **Multiple mechanisms of reinitiation on bicistronic**
812 **calicivirus mRNAs.** *Mol Cell* 2015, **57:**1059-1073.
813 39. Lomakin IB, Stolboushkina EA, Vaidya AT, Zhao C, Garber MB, Dmitriev SE, Steitz TA:
814 **Crystal Structure of the Human Ribosome in Complex with DENR-MCT-1.** *Cell Rep*
815 2017, **20:**521-528.
816 40. Rehfeld F, Eitson JL, Ohlson MB, Chang TC, Schoggins JW, Mendell JT: **CRISPR screening**
817 **reveals a dependency on ribosome recycling for efficient SARS-CoV-2 programmed**
818 **ribosomal frameshifting and viral replication.** *Cell Rep* 2023, **42:**112076.
819 41. Sonobe Y, Aburas J, Krishnan G, Fleming AC, Ghadge G, Islam P, Warren EC, Gu Y, Kankel
820 MW, Brown AEX, et al: **A C. elegans model of C9orf72-associated ALS/FTD uncovers a**
821 **conserved role for eIF2D in RAN translation.** *Nat Commun* 2021, **12:**6025.
822 42. Castelo-Szekely V, Arpat AB, Janich P, Gatfield D: **Translational contributions to tissue**
823 **specificity in rhythmic and constitutive gene expression.** *Genome Biol* 2017, **18:**116.
824 43. Knuckles P, Carl SH, Musheev M, Niehrs C, Wenger A, Bühler M: **RNA fate determination**
825 **through cotranscriptional adenosine methylation and microprocessor binding.** *Nat*
826 *Struct Mol Biol* 2017, **24:**561-569.
827 44. Flemr M, Bühler M: **Single-Step Generation of Conditional Knockout Mouse Embryonic**
828 **Stem Cells.** *Cell Rep* 2015, **12:**709-716.
829 45. Salmon P, Trono D: **Production and titration of lentiviral vectors.** *Curr Protoc Hum Genet*
830 2007, **Chapter 12:**Unit 12.10.
831 46. Lavery DJ, Schibler U: **Circadian transcription of the cholesterol 7 alpha hydroxylase**
832 **gene may involve the liver-enriched bZIP protein DBP.** *Genes Dev* 1993, **7:**1871-1884.
833 47. Arpat AB, Liechti A, De Matos M, Dreos R, Janich P, Gatfield D: **Transcriptome-wide sites**
834 **of collided ribosomes reveal principles of translational pausing.** *Genome Res* 2020,
835 **30:**985-999.
836 48. Martin M: **Cutadapt removes adapter sequences from high-throughput sequencing**
837 **reads.** *EMBnetjournal* 2011, **17:**10-12.
838 49. Langmead B, Salzberg SL: **Fast gapped-read alignment with Bowtie 2.** *Nat Methods* 2012,
839 **9:**357-359.
840 50. Dobin A, Davis CA, Schlesinger F, Drenkow J, Zaleski C, Jha S, Batut P, Chaisson M,
841 Gingeras TR: **STAR: ultrafast universal RNA-seq aligner.** *Bioinformatics* 2013, **29:**15-21.
842 51. Pertea M, Pertea GM, Antonescu CM, Chang TC, Mendell JT, Salzberg SL: **StringTie**
843 **enables improved reconstruction of a transcriptome from RNA-seq reads.** *Nat*
844 *Biotechnol* 2015, **33:**290-295.
845 52. Robinson MD, Oshlack A: **A scaling normalization method for differential expression**
846 **analysis of RNA-seq data.** *Genome Biol* 2010, **11:**R25.
847 53. Chothani S, Adami E, Ouyang JF, Viswanathan S, Hubner N, Cook SA, Schafer S, Rackham
848 OJL: **deltaTE: Detection of Translationally Regulated Genes by Integrative Analysis of**
849 **Ribo-seq and RNA-seq Data.** *Curr Protoc Mol Biol* 2019, **129:**e108.
850

851 # Figure Legends

852 **Figure 1. DENR is a re-initiation factor that promotes translation of hundreds of uORF-containing**
853 **transcripts, including *Klhdc8a* and *Asb8*.**
854 **(A)** Immunoblot analysis of NIH/3T3 cells confirms DENR and eIF2D depletion upon lentiviral transduction
855 with *Denr* or *Eif2d* shRNAs as compared to scramble (Scr) shRNA and *Eif2d* non-functional (nf) shRNA. β-
856 tubulin serves as loading control.
857 **(B)** Scatter plot of changes between *Denr* shRNA and control shRNA treated cells for RNA abundances vs.
858 translation efficiencies (RPF counts/RNA counts), based on ribosome profiling and RNA-seq experiments.
859 Evaluation is based on *Denr* shRNA (triplicates) and two independent control shRNAs (triplicates each).
860 mRNAs with significant change for TE are represented in green and mRNAs with significant change for RNA
861 abundance are represented in olive (adjusted p-values < 0.10, Wald test followed by FDR adjustment). Position
862 of *Asb8* and *Klhdc8a* are indicated.
863 **(C)** Violin plot showing 5′ UTR lengths of all expressed transcripts (n = 9203, grey) vs. transcripts with lower
864 TE upon *Denr* depletion (n = 221, green). DENR-responsive genes have longer 5′ UTRs (median = 260 nt)
865 than overall expressed transcripts (median = 153 nt) (p = 1.12e-14, Kolmogorov–Smirnov test).
866 **(D)** Analysis of proportion of transcripts with at least one translated uORF. The transcripts with lower TE upon
867 *Denr* depletion are enriched for translated uORFs. For all expressed transcripts (n = 9266), 3430 carry a
868 translated uORF, whereas 3370 have a uORF sequence that is non-translated and 2465 have no uORF at all.
869 In *Denr* shRNA cells, transcripts with significantly reduced TE (n = 179 after removal of transcripts with
870 ambiguous/several expressed 5′ UTRs), 156 have translated uORFs vs. 13 non-translated uORFs and 10 no
871 uORF (p-value < 1e-5, Fisher's exact test).
872 **(E)** The uORF length distribution of transcripts with reduced TE in *Denr* shRNA transduced cells (n = 522) is
873 similar to that of all expressed transcripts (n = 7811) (p-value = 0.3717, Kolmogorov-Smirnov test).
874 **(F)** Mapped footprint A-sites of *Klhdc8a* and *Asb8* transcripts in control and *Denr* knock-down cells. Read
875 counts were normalized to library depth by subsampling and replicates were merged for increased coverage.
876 **(G)** Quantification of translation efficiencies on the coding sequence for *Klhdc8a* and *Asb8* in cells treated
877 with shRNAs targeting *Denr* (green) or controls (Scramble, Scr in dark grey; non-functional *Eif2d*-targeting
878 shRNA, nf, in light grey); *Klhdc8a*: p = 0.01 and *Asb8*: p = 2.81e-3, two-tailed unpaired *t*-test.
879 **(H)** Schematic of the *Klhdc8a* 5′ UTR reporters used for the *in vivo* and *in vitro* translation assays. The 'no
880 uORF reporter' serves to evaluate the regulation by the 5′ UTR in the absence of a uORF (100 % signal). The
881 'overlapping uORF reporter' can only produce luciferase signal through leaky scanning. Comparison of the
882 WT reporter, containing the relevant uORF, with the two former reporters allows to specifically calculate re-
883 initiation. Not depicted: all plasmids also express Renilla luciferase for internal normalization.
884 **(I)** Normalized luminescence signal (firefly/Renilla) of the *Klhdc8a* reporters after transduction in WT and
885 *Denr* KO HeLa cells. The canonical initiation signal of the 'no uORF reporter' was set to 100 % in WT and
886 *Denr* KO cells individually. The shaded boxes represent the signal that can be calculated for uORF inhibition
887 (grey; 'no uORF' signal minus 'WT uORF' signal), re-initiation (blue; 'WT uORF' signal minus 'overlapping

888 uORF' signal) and leaky scanning (pink; 'overlapping uORF' signal) (significance calculated using two-tailed
889 unpaired *t*-test).
890 **(J)** Western Blot analysis of WT, *Denr* KO and *Eif2d* KO HeLa cells validates depletion of KLHDC8A in the
891 absence of DENR. U2AF65 serves as loading control.
892 **(K)** Schematic representation of ribosomal fluxes on *Klhdc8a* 5′ UTR estimated from the results shown in
893 panel (I).

894 **Figure 2. *In vitro* translation of *Klhdc8a* and *Asb8* reporters recapitulates regulation *in vivo*.**
895 **(A)** Outline of the preparation of HeLa translation-competent extracts and of the capped RNA reporters for the
896 *in vitro* translation assays. The RNA for Renilla reporter was consistently used in all *in vitro* assays for
897 normalization purposes.
898 **(B)** Immunoblot analysis of proteins extracted from HeLa cells, i.e. whole cell lysate, supernatant and pellet
899 post-dual-centrifugation and translation-competent extract post-translation. MCTS1, DENR, eIF2D and
900 RPL23 are consistently recovered in the translation-competent extracts.
901 **(C)** Immunoblot analysis of whole HeLa cell lysate and translation-competent extracts after *in vitro* translation
902 reveals increased eIF2α-p51 during the *in vitro* translation reaction. β-tubulin serves as loading control.
903 **(D)** Raw luminescence signals of firefly and Renilla luciferase reporters after *in vitro* translation in HeLa
904 translation-competent extracts complemented with or without GADD34Δ1-240 validates reduced translation
905 efficiency upon eIF2α phosphorylation.
906 **(E)** Normalized luminescence signal (firefly/Renilla) of the *Klhdc8a* reporters after *in vitro* translation in WT
907 and *Denr* KO HeLa lysates (left) and rescue assay with 0.5 μM recombinant MCTS1-DENR (right); 'no uORF
908 reporter' signal was set to 100 % and uORF inhibition, re-initiation and leaky scanning were calculated as
909 indicated by the shaded boxes and as in Fig. 1I (significance between 'WT uORF' signal in WT HeLa lysate
910 and 'WT uORF' signal in *Denr* KO lysate calculated using two-tailed unpaired *t*-test). The lower and upper
911 boundaries of the boxes correspond to the first and third quartiles while the middle line represents the median.
912 The upper and lower whiskers extend to the largest and lowest values, limited to values that are not more
913 distant than 1.5× the distance between the first and third quartiles.
914 **(F)** Schematic representation of ribosomal fluxes on *Klhdc8a* 5′ UTR reporter estimated from the results shown
915 in panel (E).
916 **(G)** As in (E), but for the *Asb8* reporters.
917 **(F)** As in (F) for the *Asb8* 5′ UTR in *vitro* data shown in (G).
918 **(I)** Normalized luminescence signal (firefly/Renilla) of the *Klhdc8a* reporters with mutated uORF penultimate
919 codon (GTG to GTC or GCG) reveals the effect of penultimate codon identity on DENR-dependence.
920 **(J)** Normalized luminescence signal (firefly/Renilla) of the *Asb8* reporters with inserted codon (TGT or GCG)
921 between the uORF start and stop codons indicates that lengthening of the uORF decreases DENR-dependence.

922 **Figure 3. eIF2α phosphorylation status moderately affects re-initiation rate of start-stop uORF and**
923 **longer uORF reporters.**

924 **(A)** Normalized luminescence signal of *Klhdc8a* reporters after *in vitro* translation in WT and *Denr* KO HeLa
925 extracts complemented with 16 ng/µl recombinant GADD34Δ1-240 (left) or without GADD34Δ1-240 (right)
926 (significance calculated using two-tailed unpaired *t*-test).
927 **(B)** Schematic representation of ribosomal fluxes on *Klhdc8a* 5′ UTR *in vitro* estimated from the results shown
928 in panel (A). Quantifications in presence of GADD34Δ1-240 are shown in black and without GADD34Δ1-
929 240 in blue.
930 **(C)** As in (A) for *Asb8* reporters.
931 **(D)** As in (B) for *Asb8* reporter data shown in (C).

932 **Figure 4. No evidence for eIF2D uORF re-initiation activity *in vivo* but low activity *in vitro*.**
933 **(A)** Schematic representation of human MCTS1-DENR and eIF2D proteins, with domains indicated. The
934 relevant amino acids positions defining the domains are specified.
935 **(B)** Distribution of ribosomes on 5′ UTR relative to CDS in *Denr* knock-down (in green) or *Eif2d* knock-down
936 (in blue) vs. control cells (n = 4242). *Denr* knock-down cells show a strong redistribution of ribosomes from
937 CDS to 5′ UTR whereas the effect is milder but still significant for *Eif2d* knock-down cells (p-values calculated
938 using Wilcoxon signed rank test).
939 **(C)** Scatter plot of changes between *Eif2d* shRNA and control cells for RNA abundances vs. translation
940 efficiencies (RPF counts/RNA counts), based on ribosome profiling and RNA-seq experiments. Evaluation is
941 based on two independent *Eif2d* shRNAs (triplicates each) and two independent control shRNAs (triplicates
942 each). mRNAs with significant change on TE were represented in blue and mRNAs with significant change
943 on RNA abundance were represented olive green (adjusted p-values < 0.10, Wald test followed by FDR
944 adjustment). Positions of *Asb8*, *Klhdc8a*, *Hoxa3*, *Med23*, *Rps20*, *Ndc80* and *Cenpa* are indicated.
945 **(D)** Analysis of proportion of transcripts with at least one translated uORF. The transcripts with lower TE upon
946 *Eif2d* depletion are not enriched for translated uORFs. For all expressed transcripts (n = 9266), 3430 carry a
947 translated uORF, whereas 3370 have a uORF sequence that is non-translated and 2465 have no uORF at all.
948 In *Eif2d* shRNA cells, transcripts with significantly reduced TE (n = 58 after removal of transcripts with
949 ambiguous/several expressed 5′ UTRs), 19 have translated uORFs vs. 19 non-translated uORFs and 20 no
950 uORF (p-value = 0.59, Fisher's exact test).
951 **(E)** Quantification of translation efficiencies on the coding sequence of selected transcripts with lower TE upon
952 *Eif2d* depletion in control and *Eif2d*-depleted cells (p-values calculated using a two-tailed unpaired *t*-test).
953 **(F)** Normalized luminescence signal (firefly/Renilla) of lentivirally transduced reporters with 5′ UTRs of
954 selected transcripts with lower TE upon *Eif2d* depletion (significance calculated using two-tailed unpaired *t*-
955 test). The signal of individual reporter expressed in WT cells was set to 100 %.
956 **(G)** Normalized luminescence signal (firefly/Renilla) of the *Asb8* reporters after *in vitro* translation in WT and
957 *Eif2d* KO HeLa extracts (p-value calculated using two-tailed unpaired *t*-test).
958 **(H)** Normalized luminescence signal (firefly/Renilla) of the *Klhdc8a* reporters after *in vitro* translation in WT
959 and *Eif2d* KO HeLa extracts (left), supplemented with 0.5 µM recombinant eIF2D (middle) or supplemented
960 with 0.5 µM of recombinant MCTS1-DENR (right, p-values calculated using two-tailed unpaired *t*-test).

961 **(I)** Normalized luminescence signal (firefly/Renilla) of the *Klhdc8a* reporters after *in vitro* translation in WT
962 and *Denr* KO HeLa extracts (left) or supplemented with 0.5 μM recombinant eIF2D (right); p-value calculated
963 using two-tailed unpaired *t*-test.
964 **(J)** Normalized luminescence signal (firefly/Renilla) of the *Klhdc8a* reporters after *in vitro* translation in WT
965 and *Denr / Eif2d* double KO HeLa extracts (left), supplemented with 0.5 μM recombinant eIF2D (middle) or
966 supplemented with 0.5 μM recombinant MCTS1-DENR (right); p-values calculated using two-tailed unpaired
967 *t*-test.
968 **(K)** Normalized luminescence signal (firefly/Renilla) of the *Klhdc8a* reporters after *in vitro* translation in WT
969 and *Eif2d* KO HeLa extracts treated with GADD34Δ1-240 (left), without GADD34Δ1-240 (middle), or
970 without GADD34Δ1-240 and complemented with 0.5 μM eIF2D (right); p-values calculated using two-tailed
971 unpaired *t*-test.

972 **Figure 5. MCTS2 interacts with DENR *in vivo* and promotes re-initiation *in vitro.***
973 **(A)** Schematic representation of endogenous DENR tagged with 3×FLAG-NeonGreen-dTAG. Treatment with
974 the dTAG-13 ligand targets DENR-3×FLAG-NeonGreen-dTAG to proteasomal degradation.
975 **(B)** Genotyping PCR analysis of *Denr*-tagged clones validates the insertion of the 3×FLAG-NeonGreen-dTAG
976 cassette upstream of *Denr* stop codon. Tagged *Denr* amplicon has a length of 2067 bp and WT *Denr* of 885
977 bp.
978 **(C)** Western Blot analysis of NIH/3T3 DENR-3×FLAG-NeonGreen-dTAG cells treated for 7 or 14 h with 500
979 nM dTAG-13 shows complete depletion of DENR upon treatment. Asterisk indicates a non-specific band that
980 migrates at a similar height of the tagged protein.
981 **(D)** Mass spectrometry analysis of proteins co-immunoprecipitated with endogenously tagged DENR in non-
982 treated vs. dTAG-13-treated cells reveals the interaction of MCTS2 with DENR. Only DENR and significant
983 hits enriched in non-treated cells are shown (p-values calculated using two-tailed unpaired *t*-test followed by
984 correction for multiple testing).
985 **(E)** Normalized RNA abundances and ribosome footprints of *Denr*, *Mcts1* and *Mcts2* in control and *Denr*
986 depleted NIH/3T3 cells (p-values calculated using two-tailed unpaired *t*-test).
987 **(F)** Alignment of human, rhesus macaque, mouse and rat MCTS1 and MCTS2 amino acid sequences. The
988 amino acids changing relative to mouse MCTS1 are highlighted with colors according to their side-chain
989 chemistry.
990 **(G)** Structural model of MCTS1-DENR (turquoise/green) in interaction with the 40S ribosomal subunit (grey),
991 Met-tRNA$^{Met}_{i}$ (magenta) and an mRNA shown schematically (orange). The amino acids that undergo changes
992 in MCTS2 are indicated in red in the structure and labeled. PDB accession numbers used for depiction: 5vyc
993 (40S and MCTS1-DENR), 5oa3 (initiator tRNA), 6ms4 (MCTS1-interacting domain of DENR)
994 **(H)** Normalized luminescence signal (firefly/Renilla) of the *Klhdc8a* reporters after *in vitro* translation in WT
995 and *Denr* KO HeLa lysates (left), substituted with 0.5 μM of recombinant DENR, MCTS1-DENR or MCTS2-
996 DENR as indicated (p-values calculated using two-tailed unpaired *t*-test).
997 **(I)** As in (H), for the *Asb8* reporters.

998 ## Supplementary Figure Legends

999 **Supplementary Figure 1. *Klhdc8a* and *Asb8* both contain a single AUG uORF that is conserved across**
1000 **mammals.**

1001 **(A)** Nucleotide sequences of mouse *Klhdc8a* 5′ UTR and beginning of CDS. Position and amino acid sequence
1002 of uORF and CDS are shown and highlighted in colors.

1003 **(B)** As in (A), but for *Asb8* 5′ UTR and beginning of CDS.

1004 **(C)** Sequence alignments of the 3′ portion of the 5′ UTR of *Klhdc8a* from rat, mouse, rabbit, gorilla, human,
1005 pig and lion show good conservation of their uORF sequences.

1006 **(D)** As in (C) for *Asb8*.

1007 **Supplementary Figure 2. Shortening of *Klhdc8a* 5′ UTR increases the raw luciferase signal without**
1008 **affecting the re-initiation rate.**

1009 **(A)** Schematic representation of the short and long 5′ UTR of *Klhdc8a* and the whole 5′ UTR of *Asb8* WT
1010 reporters used in this study compared to the mouse *Atf4* transcript. uORF lengths, upstream and downstream
1011 sequence lengths and GC contents are indicated.

1012 **(B)** Raw luminescence signal of long vs. short 5′ UTRs of *Klhdc8a* reporters after *in vitro* translation in HeLa
1013 WT lysate shows higher signal upon shortening of the 5′ UTR.

1014 **(C)** Normalized luminescence signal (firefly/Renilla) of the *Klhdc8a* reporters after *in vitro* translation in WT
1015 and *Denr* KO HeLa lysates of the short 5′ UTR reporters (left) and the long 5′ UTR reporters (right, significance
1016 calculated using two-tailed unpaired *t*-test)

1017 **Supplementary Figure 3. Effect of tunicamycin treatment on *Klhdc8a* reporter *in vivo*.**

1018 **(A)** Western blot analysis of whole cell protein extracts or translation-competent extracts before and after *in*
1019 *vitro* translation, non-treated or treated with 1 µg/ml tunicamycin or with 16 ng/µl GADD34Δ1-240, reveals
1020 that eIF2α-p51 phosphorylation level increase is stronger in *in vitro* translation reactions without GADD34Δ1-
1021 240 than after tunicamycin-mediated ISR induction.

1022 **(B)** Normalized luminescence signal (firefly/Renilla) of *Klhdc8a* reporters after transduction in WT and *Denr*
1023 KO cells non-treated (left) and treated with tunicamycin (right).

1024 **(C)** Schematic representation of ribosomal fluxes on *Klhdc8a* 5′ UTR estimated from the results shown in
1025 panel (B). Values measured in non-treated cells are shown in black and those quantified from tunicamycin-
1026 treated cells in blue.

1027 **(D)** Normalized *in vivo* translation signal (firefly/Renilla) of *Atf4* and *Atf5* reporters measured in transduced
1028 HeLa WT and tunicamycin-treated cells confirms the increased translation of the two reporters upon eIF2α
1029 phosphorylation.

1030 **Supplementary Figure 4. Ribosome profiling and *in vivo* dual luciferase assay reveals differential effects**
1031 **of *Denr* and *Eif2d* knock-down.**

1032 **(A)** Venn diagram of transcripts with reduced TE upon *Denr* or *Eif2d* knock-down shows that only one
1033 transcript overlaps between the two groups.

1034 **(B)** Correlation analysis between translation efficiency in *Denr* and *Eif2d* knock-down cells shows a weak but
1035 significant correlation (Pearson correlation = 0.1339, p-value < 2.2e-16).
1036 **(C)** Violin plot of 5′ UTR lengths of all expressed transcripts (n = 9203, grey) vs. transcripts with lower TE
1037 upon *Denr* depletion (n = 221, green) and *Eif2d* depletion (n = 73, blue). eIF2D-responsive genes tend to have
1038 a shorter 5′ UTR (median = 110 nt) than overall expressed transcripts (median = 153 nt) (p = 0.09,
1039 Kolmogorov–Smirnov test).
1040 **(D)** Cumulative distributions of transcript per kilobase million (TPM) of all expressed transcripts, transcripts
1041 with decreased TE upon *Eif2d* knock-down and transcripts with decreased TE upon *Denr* knock-down show a
1042 strong enrichment for highly abundant transcripts among eIF2D-responsive mRNAs (p-value calculated using
1043 the Kolmogorov–Smirnov test).
1044 **(E)** Gene Ontology analysis of transcripts with decreased TE upon *Eif2d* depletion (p-values adjusted for
1045 multiple tests using FDR).
1046 **(F)** Cumulative distributions of TPM of all expressed transcripts, transcripts with changed abundance upon
1047 *Eif2d* knock-down and transcripts with changed abundance upon *Denr* knock-down show an enrichment for
1048 highly abundant transcripts among eIF2D-responsive mRNAs (p-value calculated using the Kolmogorov–
1049 Smirnov test).
1050 **(G)** Gene Ontology analysis of transcripts with increased abundance upon *Eif2d* depletion (p-values adjusted
1051 for multiple tests using FDR).
1052 **(H)** Gene Ontology analysis of transcripts with decreased abundance upon *Eif2d* depletion (p-values adjusted
1053 for multiple tests using FDR).
1054 **(I)** Cell proliferation analysis of NIH/3T3 cells transduced with scramble shRNA, nf *Eif2d* shRNA, *Denr*
1055 shRNA and *Eif2d* shRNAs shows that a larger fraction of *Eif2d* knock-down cells are found in the G1 phase
1056 of the cell cycle than is the case across control cells or *Denr*-depleted cells (p-values calculated using two-
1057 tailed unpaired *t*-test).
1058 **(J)** Normalized luminescence signals (firefly/Renilla) of *Klhdc8a* reporters after transduction in HeLa WT and
1059 *Eif2d* KO cells show no change in re-initiation rates upon *Eif2d* depletion (p-values calculated using two-tailed
1060 unpaired *t*-test).

1061 **Supplementary Figure 5. Alignment of mouse *Mcts1* and *Mcts2* coding sequences.**
1062 **(A)** Nucleotide alignment of *Mcts1* and *Mcts2* coding sequences from *Mus musculus*.

1063 **Supplementary Figure 6. DENR depletion leads to an accumulation of ribosomes at the uORF stop**
1064 **codon on the endogenous *Atf4* transcript.**
1065 **(A)** Mapped footprint A-sites of mouse *Atf4* transcripts in control, *Eif2d* and *Denr* knock-down cells. Read
1066 numbers were normalized to library depth by subsampling and replicates were merged for increased coverage.

1067 **Supplementary Figure 7. *Mcts2* expression in mouse liver and kidney.**

1068 **(A)** RPKM of *Denr*, *Mcts1* and *Mcts2* around-the-clock in mouse liver and kidney confirms expression of
1069 *Mcts2* in adult mice. Liver and kidney RNA-seq and Ribo-seq data were taken from previously published
1070 studies [25, 42].

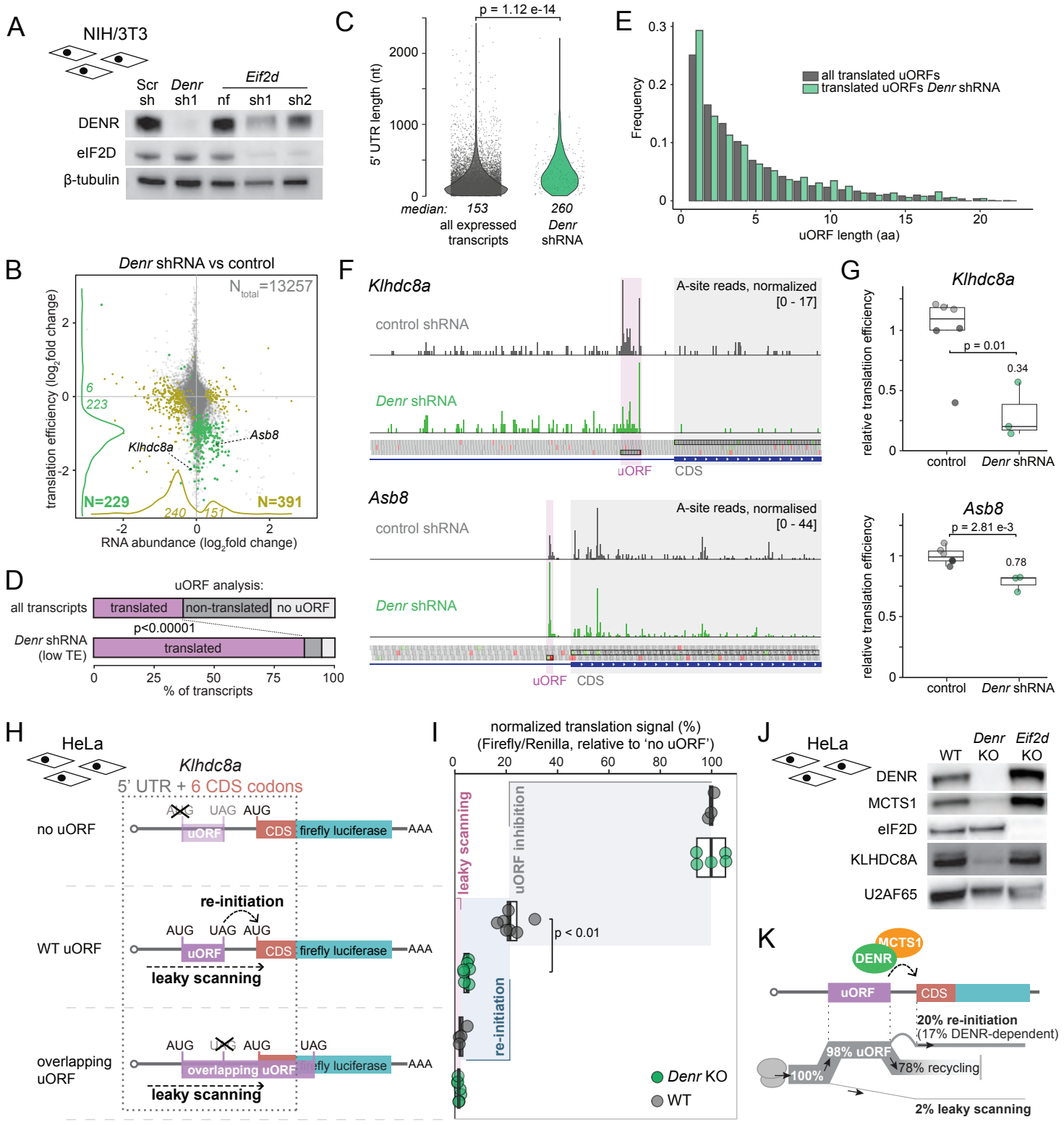
A
NIH/3T3
Scr sh
Denr sh1
Eif2d
nf
sh1
sh2
DENR
eIF2D
β-tubulin
C
p = 1.12 e-14
5' UTR length (nt)
median: 153
260
all expressed transcripts
Denr shRNA
E
Frequency
all translated uORFs
translated uORFs Denr shRNA
uORF length (aa)
B
Denr shRNA vs control
N total =13257
translation efficiency (log2 fold change)
RNA abundance (log2 fold change)
Klhdc8a
Asb8
N=229
N=391
D
uORF analysis:
all transcripts
translated
non-translated
no uORF
p<0.00001
Denr shRNA (low TE)
% of transcripts
F
Klhdc8a
A-site reads, normalized [0 - 17]
control shRNA
Denr shRNA
uORF
CDS
Asb8
A-site reads, normalised [0 - 44]
G
Klhdc8a
p = 0.01
0.34
relative translation efficiency
control
Denr shRNA
Asb8
p = 2.81 e-3
0.78
H
HeLa
Klhdc8a
5' UTR + 6 CDS codons
no uORF
WT uORF
overlapping uORF
re-initiation
leaky scanning
firefly luciferase
AAA
I
normalized translation signal (%)
(Firefly/Renilla, relative to 'no uORF')
leaky scanning
uORF inhibition
re-initiation
p < 0.01
Denr KO
WT
J
HeLa
WT
Denr KO
Eif2d KO
DENR
MCTS1
eIF2D
KLHDC8A
U2AF65
K
MCTS1
DENR
uORF
CDS
20% re-initiation
(17% DENR-dependent)
98% uORF
100%
78% recycling
2% leaky scanning

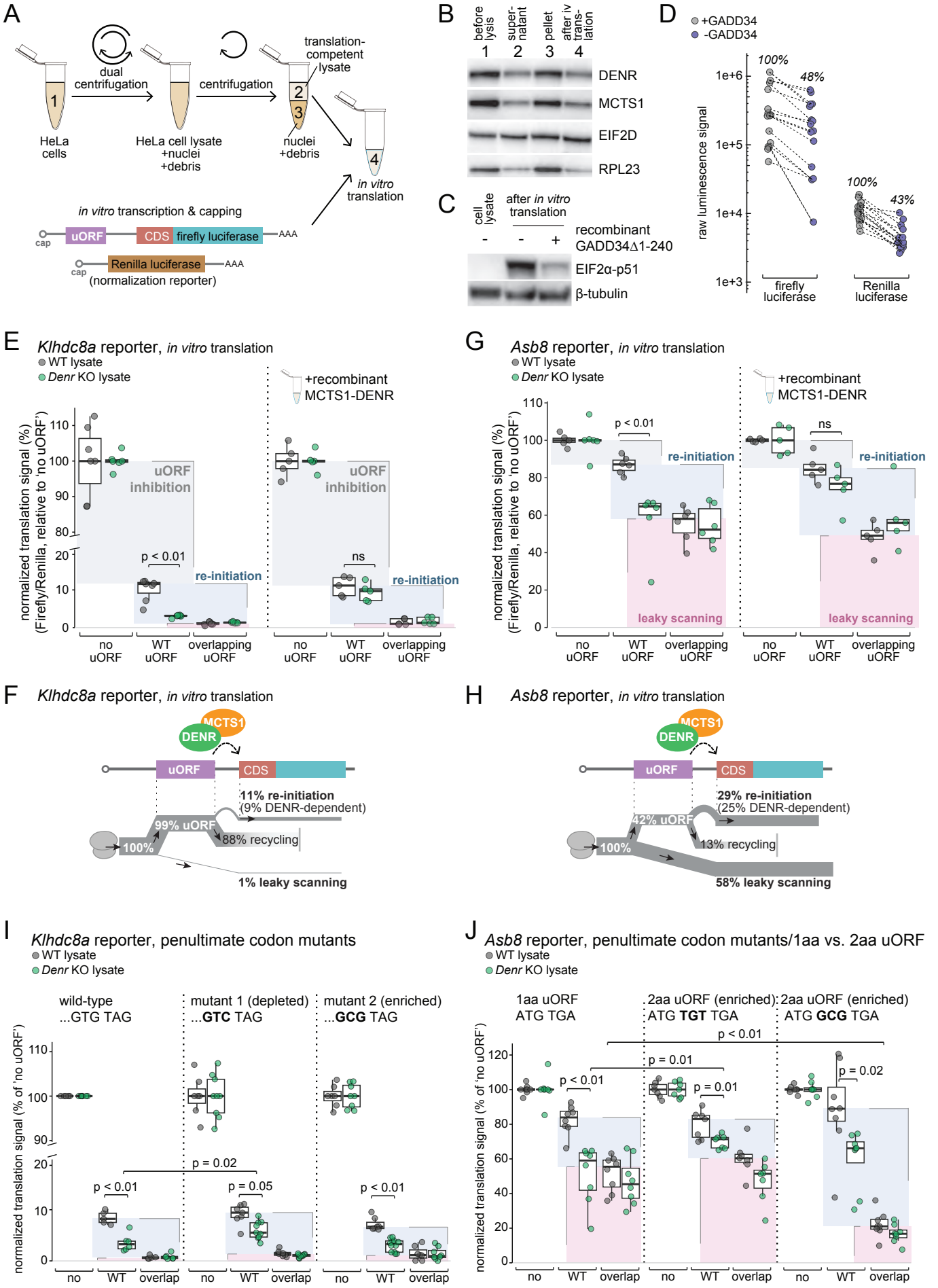
A
dual centrifugation
centrifugation
translation-competent lysate
HeLa cells
HeLa cell lysate +nuclei +debris
nuclei +debris
in vitro translation
in vitro transcription & capping
cap
uORF
CDS
firefly luciferase
AAA
Renilla luciferase
(normalization reporter)
B
before lysis
super-natant
pellet
after iv trans-lation
DENR
MCTS1
EIF2D
RPL23
C
cell lysate
after in vitro translation
recombinant GADD34Δ1-240
EIF2α-p51
β-tubulin
D
+GADD34
-GADD34
raw luminescence signal
100%
48%
43%
firefly luciferase
Renilla luciferase
E
Klhdc8a reporter, in vitro translation
WT lysate
Denr KO lysate
+recombinant MCTS1-DENR
normalized translation signal (%) (Firefly/Renilla, relative to 'no uORF')
uORF inhibition
re-initiation
p < 0.01
ns
no uORF
WT uORF
overlapping uORF
G
Asb8 reporter, in vitro translation
leaky scanning
F
Klhdc8a reporter, in vitro translation
MCTS1
DENR
11% re-initiation
(9% DENR-dependent)
99% uORF
88% recycling
100%
1% leaky scanning
H
Asb8 reporter, in vitro translation
29% re-initiation
(25% DENR-dependent)
42% uORF
13% recycling
58% leaky scanning
I
Klhdc8a reporter, penultimate codon mutants
wild-type ...GTG TAG
mutant 1 (depleted) ...GTC TAG
mutant 2 (enriched) ...GCG TAG
normalized translation signal (% of 'no uORF')
p = 0.02
p < 0.01
p = 0.05
no
WT
overlap
J
Asb8 reporter, penultimate codon mutants/1aa vs. 2aa uORF
1aa uORF ATG TGA
2aa uORF (enriched) ATG TGT TGA
2aa uORF (enriched) ATG GCG TGA
p = 0.01
p = 0.02

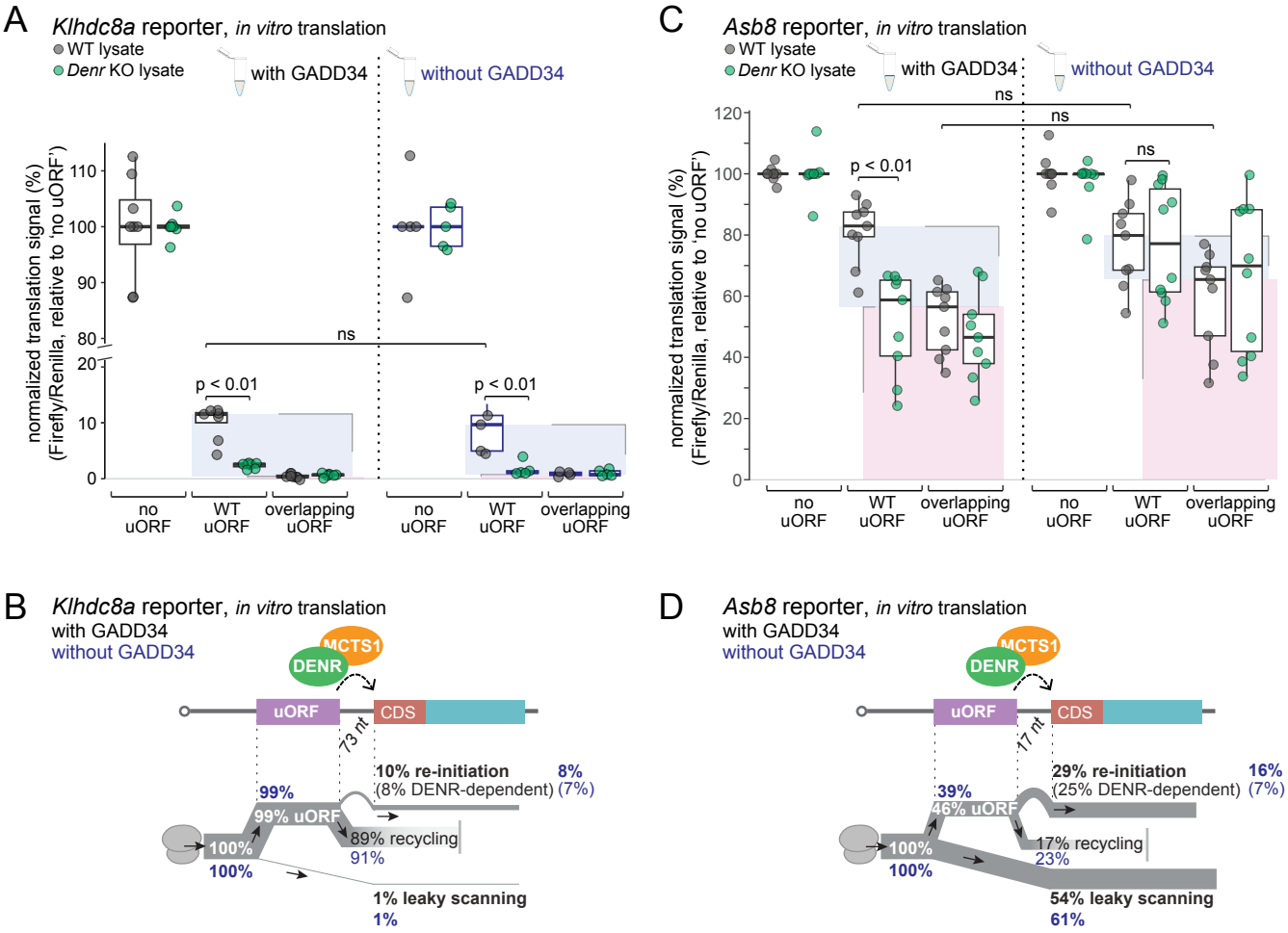
A
Klhdc8a reporter, in vitro translation
WT lysate
Denr KO lysate
with GADD34
without GADD34
normalized translation signal (%)
(Firefly/Renilla, relative to 'no uORF')
ns
p < 0.01
p < 0.01
no uORF
WT uORF
overlapping uORF
no uORF
WT uORF
overlapping uORF
C
Asb8 reporter, in vitro translation
WT lysate
Denr KO lysate
with GADD34
without GADD34
normalized translation signal (%)
(Firefly/Renilla, relative to 'no uORF')
ns
ns
ns
p < 0.01
no uORF
WT uORF
overlapping uORF
no uORF
WT uORF
overlapping uORF
B
Klhdc8a reporter, in vitro translation
with GADD34
without GADD34
MCTS1
DENR
uORF
CDS
73 nt
10% re-initiation
(8% DENR-dependent)
8%
(7%)
99%
99% uORF
100%
100%
89% recycling
91%
1% leaky scanning
1%
D
Asb8 reporter, in vitro translation
with GADD34
without GADD34
MCTS1
DENR
uORF
CDS
17 nt
29% re-initiation
(25% DENR-dependent)
16%
(7%)
39%
46% uORF
100%
100%
17% recycling
23%
54% leaky scanning
61%

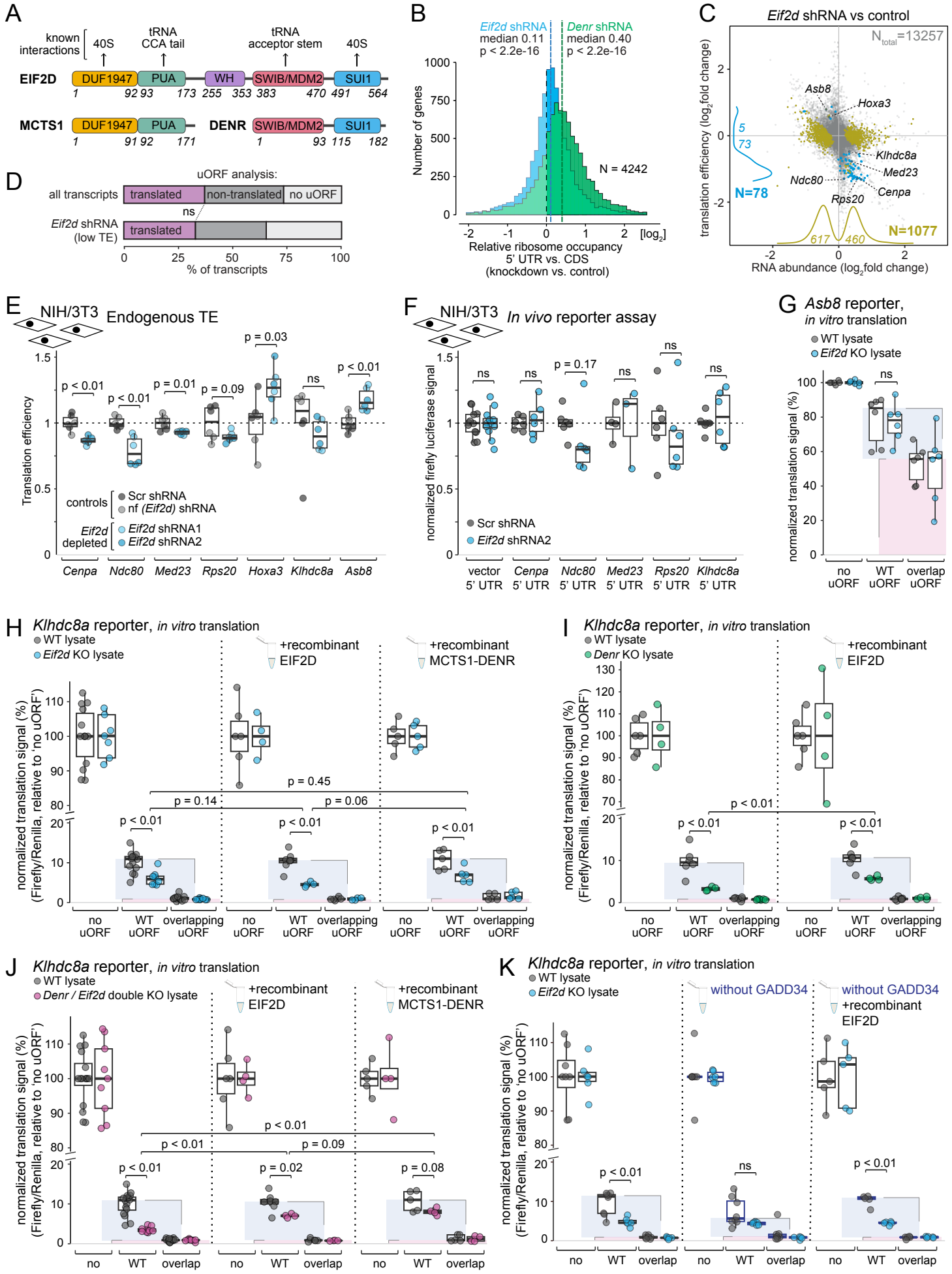
A
known interactions
40S
tRNA CCA tail
tRNA acceptor stem
40S
EIF2D
DUF1947
PUA
WH
SWIB/MDM2
SUI1
MCTS1
DENR
B
Eif2d shRNA median 0.11 p < 2.2e-16
Denr shRNA median 0.40 p < 2.2e-16
Number of genes
N = 4242
Relative ribosome occupancy 5' UTR vs. CDS (knockdown vs. control)
C
Eif2d shRNA vs control
N_total=13257
translation efficiency (log2fold change)
RNA abundance (log2fold change)
Asb8
Hoxa3
Klhdc8a
Med23
Ndc80
Cenpa
Rps20
N=78
N=1077
D
uORF analysis:
all transcripts
translated
non-translated
no uORF
Eif2d shRNA (low TE)
% of transcripts
E
NIH/3T3 Endogenous TE
Translation efficiency
controls
Scr shRNA
nf (Eif2d) shRNA
Eif2d depleted
Eif2d shRNA1
Eif2d shRNA2
Cenpa
Ndc80
Med23
Rps20
Hoxa3
Klhdc8a
Asb8
F
NIH/3T3 In vivo reporter assay
normalized firefly luciferase signal
Scr shRNA
Eif2d shRNA2
vector 5' UTR
G
Asb8 reporter, in vitro translation
WT lysate
Eif2d KO lysate
normalized translation signal (%)
no uORF
WT uORF
overlap uORF
H
Klhdc8a reporter, in vitro translation
WT lysate
Eif2d KO lysate
+recombinant EIF2D
+recombinant MCTS1-DENR
normalized translation signal (%) (Firefly/Renilla, relative to 'no uORF')
no uORF
WT uORF
overlapping uORF
I
Klhdc8a reporter, in vitro translation
WT lysate
Denr KO lysate
+recombinant EIF2D
J
Klhdc8a reporter, in vitro translation
WT lysate
Denr / Eif2d double KO lysate
+recombinant EIF2D
+recombinant MCTS1-DENR
no
WT
overlap
K
Klhdc8a reporter, in vitro translation
WT lysate
Eif2d KO lysate
without GADD34
without GADD34 +recombinant EIF2D

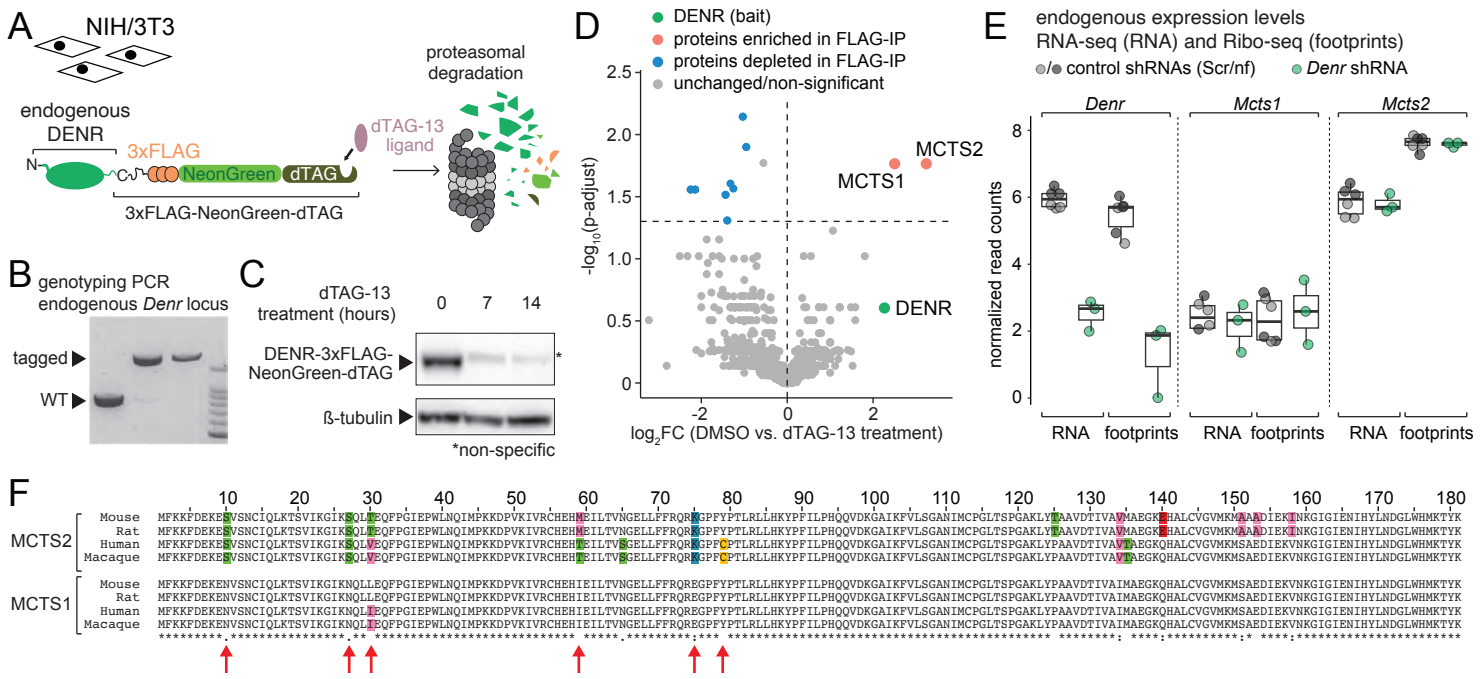
A
NIH/3T3
endogenous DENR
3xFLAG
NeonGreen
dTAG
3xFLAG-NeonGreen-dTAG
dTAG-13 ligand
proteasomal degradation
B
genotyping PCR endogenous Denr locus
tagged
WT
C
dTAG-13 treatment (hours)
0 7 14
DENR-3xFLAG-NeonGreen-dTAG
ß-tubulin
*non-specific
D
DENR (bait)
proteins enriched in FLAG-IP
proteins depleted in FLAG-IP
unchanged/non-significant
MCTS2
MCTS1
DENR
-log10 (p-adjust)
log2FC (DMSO vs. dTAG-13 treatment)
E
endogenous expression levels
RNA-seq (RNA) and Ribo-seq (footprints)
control shRNAs (Scr/nf)
Denr shRNA
Denr
Mcts1
Mcts2
normalized read counts
RNA footprints RNA footprints RNA footprints

F

MCTS2
MCTS1
Mouse
Rat
Human
Macaque

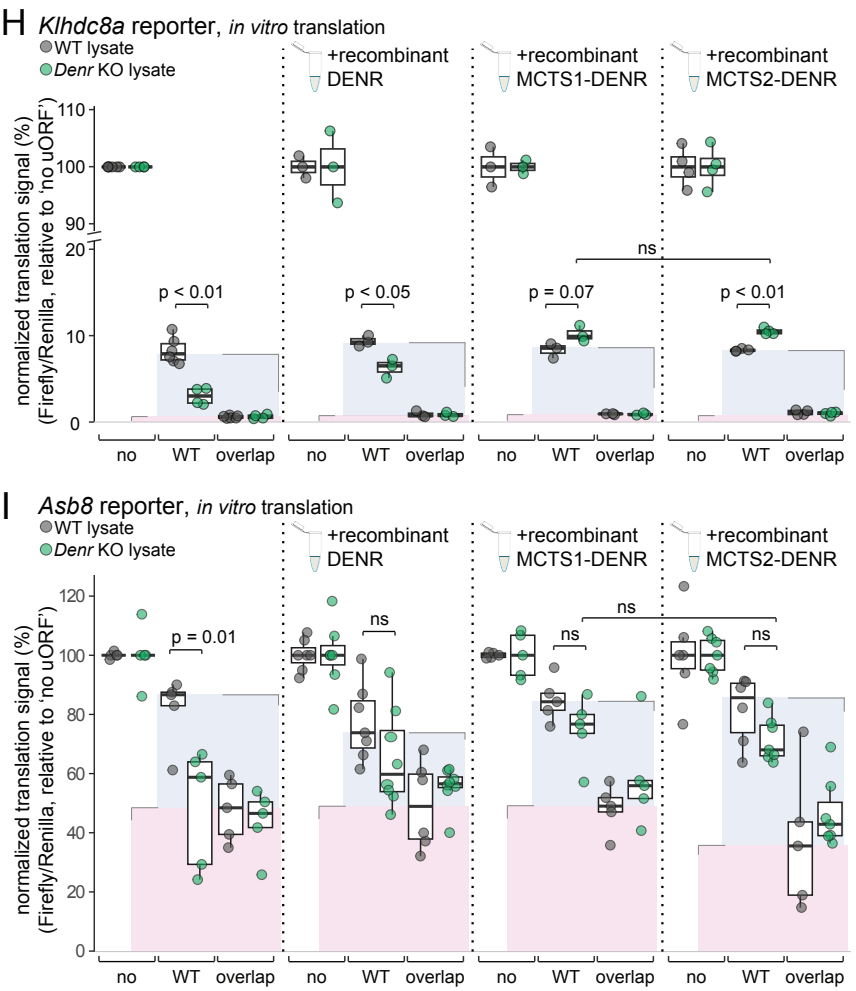
H
Klhdc8a reporter, in vitro translation
WT lysate
Denr KO lysate
+recombinant DENR
+recombinant MCTS1-DENR
+recombinant MCTS2-DENR
normalized translation signal (%) (Firefly/Renilla, relative to 'no uORF')
p < 0.01
p < 0.05
p = 0.07
p < 0.01
ns
no WT overlap
I
Asb8 reporter, in vitro translation
p = 0.01
ns

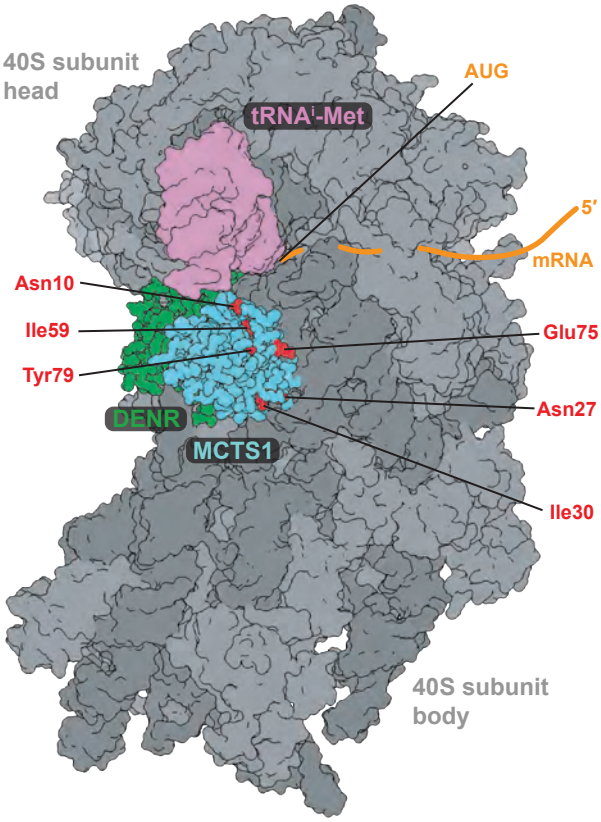
G
40S subunit head
AUG
tRNAi-Met
5'
mRNA
Asn10
Ile59
Tyr79
Glu75
Asn27
Ile30
DENR
MCTS1
40S subunit body